Peer-reviewed version available at *Quaternary* **2019**, *2*, 16; doi:10.3390/quat2020016

Review

Speleothems from the Middle East: An Example of Water Limited Environments in the SISAL Database

Yuval Burstyn [1,2], Belen Martrat [3], Jordi F. Lopez [3], Eneko Iriarte [4], Matthew J. Jacobson [5], Mahjoor Ahmad Lone [6,7], and Michael Deininger [8]

[1] Geological Survey of Israel, 30 Malchei Israel Street, Jerusalem, Israel; yuval.burstyn@mail.huji.ac.il
[2] Institute of Earth Sciences, Hebrew University of Jerusalem, Edmond Y. Safra Givat Ram Campus. Jerusalem, Israel; yuval.burstyn@mail.huji.ac.il
[3] Department of Environmental Chemistry, Spanish Council for Scientific Research (CSIC), Institute of Environmental Assessment and Water Research (IDAEA), Barcelona, Spain; belen.martrat@idaea.csic.es, jlfqam@idaea.csic.es
[4] Laboratorio de Evolución Humana, Universidad de Burgos, Burgos, Spain; eneko@me.com
[5] Department of Archaeology and Centre for Past Climate Change, University of Reading, Reading, UK; m.j.jacobson2@pgr.reading.ac.uk
[6] High-Precision Mass Spectrometry and Environment Change Laboratory (HISPEC), Department of Geosciences, National Taiwan University, Taipei, 10617, Taiwan.; lonemahjoor@gmail.com
[7] Research Center for Future Earth, National Taiwan University, Taipei 10617, Taiwan ROC
[8] Institute of Geosciences, Johannes Gutenberg University Mainz, J.-J.-Becher-Weg 21, 55128, Mainz, Germany; michael.deininger@uni-mainz.de
* Correspondence: yuval.burstyn@mail.huji.ac.il; Tel.: +972-544-331745

Abstract: The Middle East spans the transition between temperate Mediterranean climate in the Levant to hyper-arid sub-tropical deserts in the southern part of the Arabian Peninsula, with the complex alpine topography in the northeast feeding the Euphrates and Tigris rivers which support life in the southeastern Fertile Crescent (FC). Climate projections predict severe drying in major parts much of the ME in response to global warming, making it important to understand the controls of hydro-climate perturbations in the region. Here we discuss 23 ME speleothem stable oxygen isotope (δ^{18}Occ) records from 16 sites from the SISAL_v1 database, which provide a record of past hydro-climatic variability. Sub-millennial changes in ME speleothem δ^{18}Occ values primarily indicate changes in past precipitation amounts superimposed on variations of the main synoptic pattern in the region, specifically Mediterranean cyclones. The coherency (or lack thereof) between regional records is reviewed from Pleistocene to present, covering the Last Glacial Maximum (LGM), prominent events during deglaciation, and transition into the Holocene. The available speleothem δ^{18}Occ time-series are investigated by binning and normalizing at 25-year and 200-year time windows over the Holocene. Important Holocene climatic oscillations are discussed, such as the 8.2 ka, 4.2 ka and 0.7 ka (the Little Ice Age) Before Present events. Common trends in the standardized anomalies are tested against different climate archives. Finally, recommendations for future speleothem-based research in the region are given along with comments on the utility and completeness of the SISAL database.

Keywords: SISAL database; speleothem; cave; isotopes; Middle East, palaeoclimate.

1. Introduction

The Middle East (ME) has a heterogeneous climate for its size, encompassing the Eastern Mediterranean (EM, or Levant) and the Fertile Crescent (FC) (often considered in tandem,) as well as parts of the Arabian Peninsula (AP) and North-East Africa [1,2]. The region spans the transition between temperate Mediterranean climate in the Levant to hyper-arid sub-tropical deserts in the south, with complex alpine topography in the northeast feeding the Euphrates and Tigris rivers which supports life in the southeastern FC (Figure 1). Climate projections predict severe drying in

major parts of the ME in response to global warming, with a considerable impact for societies [3–5]. Climate reconstructions, and archaeological information, suggest that changes in the regional hydroclimate was a primary driver in human expansions out of Africa [6], the Neolithic revolution, and the development of the first complex societies [7]. The ME has plentiful archeological records of human settlement throughout much of the Quaternary, and well into the Holocene [8–14]. Initially, the predominantly semi to hyper-arid climate of the region served as a bottle neck for early hominin dispersion out of Africa, allowing migrations onto the Levant and the AP pathways only during wetter periods that were identified using, among other methods, speleothem growth (wet)/non-growth (dry) patterns and their respective isotopic record [15–18]. Since the Last Glacial Maximum from c. 25 to 20 ka BP (BP is Before Present, calibrated to the year 1950 of the Common Era, hereafter CE) and the following transition into the Holocene interglacial, there has been considerable evidence that variations in climate served as a driver in Homo Sapiens' cultural evolution. The most notable is the "Neolithic Revolution", where it has been suggested that with a warming post-glacial climate hunter-gatherers were able to cultivate a number of food plants [19]. Wheat, cultivated in the FC around 9500 years BP, suggests that the ME was the first region to cultivate plants and support sedentary human communities [20,21]. The ME localities, specifically the FC, were also the earliest locations where sophisticated civilizations, city-states and complex empire systems appeared during the mid- to late-Holocene [22,23]. It has been argued that the expansion and subsequent collapse of these civilizations was partly driven by rapid climate change events [14,24–28] superimposed on more gradual millennial climatic shifts. Furthermore, recent studies have suggested an association between a contemporary increase in the frequency and intensity of droughts in recent decades, to geopolitical unrest in the region, e.g. the Syrian Civil War [25,29,30]. These correlations highlight the importance of understanding both past and future climate perturbation in the ME. This can be achieved by making use of large spatio-temporal networks/datasets of terrestrial hydro-climate archives. Regional-scale coherency investigations would greatly improve our understanding of past variations in the spatio-temporal precipitation pattern of the ME, thereby resolving some of the contradictions between different records in the region [1,31].

The first version of the Speleothem Isotope Synthesis and Analysis database (SISAL_v1) [32,33], contains 376 isotope entity records derived from speleothems (secondary cave deposits) worldwide. Speleothems are commonly used as archives of past terrestrial climatic variability. This is because speleothems can be accurately dated and preserve multiple climate-sensitive proxies, which can be sampled at high spatial and temporal resolution, respectively, even under dry conditions [18,34,35]. This gives speleothem records a distinct advantage over alternative palaeoclimate proxies (e.g. lake cores, tree-rings, corals) in the ME.

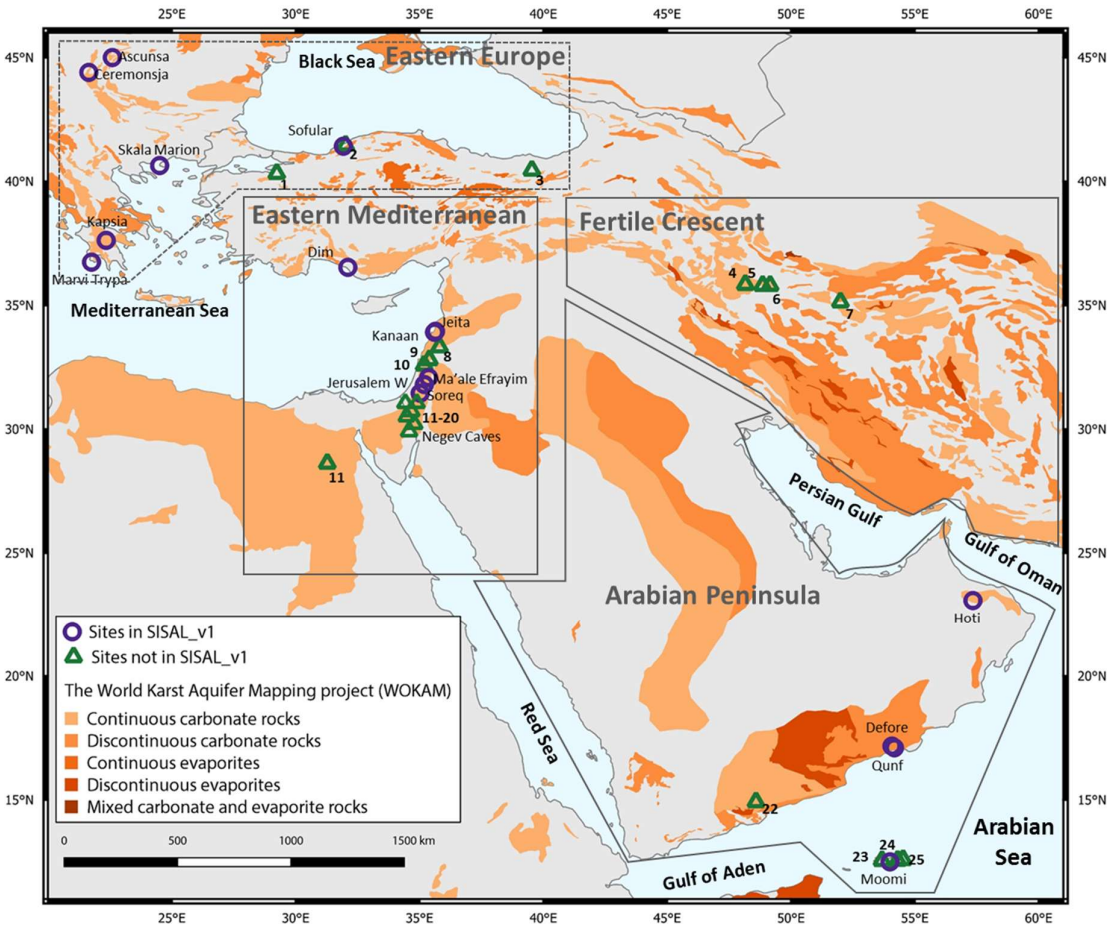

Figure 1. Location of ME speleothem records that are included in SISAL_v1 (purple circles) and other identified records, not yet included in the database (green triangles). The base map shows the distribution of carbonate and evaporite rocks in the ME, as provided by the World Karst Aquifer Mapping project (WOKAM) [36]. Cave sites with entities not included in the SISAL database are numbered (Table 1): 1) Karca 2) Ovaik 3) Akcakale 4) Katleh Khor 5) Qal'e Kord 6) Gejkar 7) Gol-e Zard 8) Mitzpe Shlagim 9) Peqiin 10) Zalmon 11) Ashalim 12) Even Sid 13) Hol-Zakh 14) Izzim 15) Ma'ale Ha-Mishar 16) Ma'ale Dargot 17) Makhtesh ha-Qatan 18) Shizfon mini-caves 19) Tzavoa 20) Wadi Lotz 21) Wadi Sannur 22) Mukalla 23) Dimarshim 24) Casecas 25) Hoq.

In this work we review 20 speleothem isotope records (hereafter entities) that are in SISAL_v1 for the ME, which includes sites in Lebanon, Israel, The West Bank, Oman, Yemen, and southeast Turkey. Additional 6 sites from Eastern Europe and northern Turkey (see Kern et al. [37,38]), are included as these sites are along the dominant EM storm tracks, the major climate patterns controlling precipitation in the region (Figures 1 and 2; Table 1). The aim of this work is to highlight the applicability of speleothems from the ME currently logged in the SISAL_v1 database to resolve regional-scale consistencies and inconsistencies and to test for spatial coherency between speleothems and additional climate recorders (i.e. Arctic ice sheets and Mediterranean surface temperatures). The available δ^{18}Occ Holocene time-series are investigated via binning and normalizing (providing median, the 25- and 75-qunatile of the data) at 25-year and 200-year time windows, as used previously in the context of the PAGES 2k databases [39]. This method is used to better understand how different Holocene events, detected regionally, are differentiated with the context of a regional composite analysis (i.e. Sapropel 1, the 8.2 ka and the 4.2 ka event or the Little Ice Age at 0.7 ka BP). Finally, recommendations for future speleothem-based research is given, on one hand, making use of the SISAL database and on the other hand by the identification of potential regions for the generation of new speleothem proxy time-series.

Table 1. List of all speleothem records: Metadata includes: site or cave name, site of Figure 1 identification, country, latitude, longitude, elevation, entity or speleothem name and id# within each site, minimum and maximum ages given in years BP (1950), and published references. Top table: records available in SISAL_v1 (with annotations of some entities as yet to be added). Bottom table: additional sites and speleothems not included in in SISAL_v1). MIS ages stand for Marine Isotope Stage chronology [40]

site_name	*Site _id*	Country	*latitude* °N	*longitude* °E	elevation (masl)	*entity _name*	*entity _id*	Min. Age	Max. Age	Ref.
Ascunsa	72	Romania	45.00	22.60	1050	POM-2	161	-32	8169	[41]
Ceremosjna	76	Serbia	44.40	21.65	530	CC-1	165	-48	2426	[42]
Defore	170	Oman	17.17	54.08	150	S3	366	-46	731	[43]
						S4	Not in v1	9095	10,693	[44]
Dim	79	Turkey	36.53	32.11	232	Dim-E2	168	9738	13,094	[45]
						Dim-E3	169	12,575	89,714	
						Dim-E4	170	12,020	14,555	
Hoti	152	Oman	23.08	57.35	800	H5	327	6026	9607	[44,46]
						H1	Not in v1	MIS5a	6277	[44,47]
						H2		MIS1		
						H3		MIS1		
						H4		MIS5d		
						H10		MIS 1-2		
						H11		MIS 1-2		
						H12		164		
						H13		MIS 7/9		
						H14		MIS51-2		
						flowstone		MIS5e		
Jeita	11	Lebanon	33.95	35.65	100	Jeita-1	58	1137	12,288	[48,49]
						Jeita-2	59	13,330	20,367	
						Jeita-3	60	372	847	
						JeG-Stm-1	Not in v1	~1100	~11,900	[49]
Jerusalem West	68	Israel	31.80	35.20	700	AF-12	152	-16	168,714	[50]
Kanaan	19	Lebanon	33.91	35.61	98	Kanaan_MIS5	81	83,125	128,847	[51]
						Kanaan_MIS6	82	154,455	193,498	
Kapsia	44	Greece	37.62	22.35	700	GK-09-02	120	1115	2904	[52]
Ma'ale Efrayim	110	West Bank	32.08	35.37	250	ME-12	218	16,548	66,948	[18]
Mavri Trypa	156	Greece	36.74	21.76	70	S1	347	1296	4687	[53]

Preprints (www.preprints.org) | NOT PEER-REVIEWED | Posted: 6 February 2019 doi:10.20944/preprints201902.0063.v1

Peer-reviewed version available at *Quaternary* **2019**, *2*, 16; doi:10.3390/quat2020016

Moomi	138	Yemen	12.50	54.00	400	M1-5	293	11,086	27,370	[54]
						M1-2	Not in v1	~40,000	~53,000	[54]
Qunf	159	Oman	17.10	54.18	650	Q5	351	308	10,558	[44]
Skala Marion	56	Greece	40.64	24.51	41	MAR_L	136	1481	5534	[55]
Sofular	141	Turkey	41.42	31.93	700	SO-1	305	-56	50,275	[56]
						SO-2	Not in v1	-60	59,510	[57,58]
						SO-4		1080	307,030	
						SO-6		93572	133,200	
						SO-10		~present	<2500	
						SO-14B		475,910	670,000	
						SO-17A		86,190	122,930	
Soreq	160	Israel	31.45	35.03	400	Soreq composite	354	~present	30,031	[59]
						2N	353	4440	33,804	[27]
						2 – 6	352	743	2086	[14]
						Numerous	Not in v1	~present	>180	[13,24, 60–67]

Sites identified but currently not in SISAL_v1 (see Figure 1)

Cave Name	**Fig. 1 id**	**Country**	**latitude (N)**	**longitude (E)**	**elevation (masl)**	***Identified speleothems***		**Min. Age***	**Max. Age***	**Ref.**
Ashalim	11	Israel	30.94	34.74	400		-			
Akcakale	3	Turkey	40.45	39.54		2p	-	-55	189	[68]
Casecas	24	Yemen	12.56	54.31		STM5	-	12	856	[69]
Dimarshim	23	Yemen	12.55	53.68		D1	-	~present	4530	[44]
Even Sid	12	Israel	30.64	34.81	800		-			
Gejkar	6	Iraq	35.80	49.16		Gej-1	-	-63	2380	[25]
Gol-e Zard	7	Iran	35.13	52.00	2530	-	-	~3700	5100	[70]
Hol-Zakh	13	Israel	31.16	35.20	150					
Hoq	25	Yemen	12.59	54.53		Hq1	-	-50	6900	[69]
						STM1		-53	5600	
						STM6		-56	4500	
Izzim	14	Israel	31.14	35.06	500		-			
Karaca	1	Turkey	40.32	29.24		K1	-	6000	77,300	[71]
Kataleh Khor	4	Iran	35.84	48.16		(2 samples)	-	214,000	500,000	[72]
Ma'ale ha-Meyshar	15	Israel	30.49	34.93	450		-			
Ma'ale Dragot	16	Israel	31.4	35.00	300	MD (5 samples)		MIS1	MIS6	[73]
Makhtesh ha-Qatan	17	Israel	30.95	35.22	-20		-			

Preprints (www.preprints.org) | NOT PEER-REVIEWED | Posted: 6 February 2019 doi:10.20944/preprints201902.0063.v1

Peer-reviewed version available at Quaternary 2019, 2, 16; doi:10.3390/quat2020016

Mitzpe Shlagim	8	Israel/Syria	33.32	35.81	2224	MS-1 MS-2 MS-3	- 	4300 8800 8500	88,000 89,000 49,100	[74]
Mukalla Cave	22	Yemen	14.92	48.59	1500	Y99 Y97-4 Y97-5	- - -	119,141 5630 8790	358,887 185,600 233,300	[16]
Ovacik	2	Turkey	41.46	32.02		O-1	-	4472	9796	[56]
Peqiin	9	Israel	32.58	35.19	650	PEK-5 PEK-6 PEK-9 PEK-10	-	5620 24,710 47,810 55,630	6780 223,700 283,650 288,160	[67]
Qal'e Kord	5	Iran	35.80	48.86		QK 8 QK 14	-	78,104 6581	99,182 127,012	[72,75]
Shizafon mini-caves	18	Israel	30.04	35.00	400		-			
Tzavoa	19	Israel	31.20	35.20	550	TZ (13 samples)		MIS2	MIS7	[73]
Wadi Lotz	20	Israel	30.47	34.58	900		-			
Wadi Sannur	21	Egypt	28.62	31.28		WSS 1 to 6	-	136,460	188,120	[76]
Zalmon	10	Israel	32.80	35.40		ZAL-1 to ZAL-7 ZAL-11	-	5000	16,000	[77]

2. Climate of the Middle East

The ME is located within the subtropical high-pressure belt between the Northern Hemisphere tropical (Hadley cell) and the mid-latitude atmospheric circulation, which is generally associated with dry climates (i.e. the global desert belt). However, the modern climate of the Mediterranean is less arid and much milder than would be expected from its location. This is because of the interplay of Mediterranean cyclogenesis and Atlantic depressions (Figure 2).

The Mediterranean Sea is characterized by an eastward gradient of increasing salinity and Sea Surface Temperatures (SST). This temperature gradient and the cold surrounding land are key drivers for Mediterranean cyclogenesis [78]. The northern EM receives the majority of its precipitation from cyclones that are associated with eastward moving storm tracks formed in the North Atlantic, or Cyprus Lows that are formed in the EM [79]. Greece and Turkey (>38ºN) receive cyclones originating to the northwest over central Europe, and in the Gulf of Genoa [80]. The EM coastal areas receive most precipitation from eastward moving storm tracks generated inside the Mediterranean region, Cyprus low systems, when cold and dry air from continental Euro-Asia interfaces with the relatively warm Mediterranean sea [81,82]. A smaller fraction of cyclones enter from outside the Mediterranean region from the Atlantic (Figure 2B), but rarely reach all the way to the EM and FC. Only a few cyclones come from North Africa, often during less stable transition seasons in autumn and spring (Figure 2B) [83]. The semi-arid to arid FC currently receives most of its moisture during winter (98% of the precipitation occurs between October-May; [25]) from Mediterranean storm tracks [79]; while summer precipitation from tropical systems is virtually absent. The AP receives rainfall from these Mediterranean frontal systems (Dec-Mar) and from precipitation that is formed due to orographic uplift, and rarely from the Indian summer monsoon (Figure 2A) [84]. The modern climate at the southern AP is largely dependent on the annual migration of the Inter-tropical Convergence Zone (ITCZ), which reaches its northern-most position in August. During this period, the Somali Jet brings large quantities of precipitation to the

Peer-reviewed version available at Quaternary 2019, 2, 16; doi:10.3390/quat2020016

southernmost parts of the AP [85]; this is particularly important in the southwest where rainfall can occur all year round due to the orographic features of the region and moisture advected from the Red Sea [86,87].

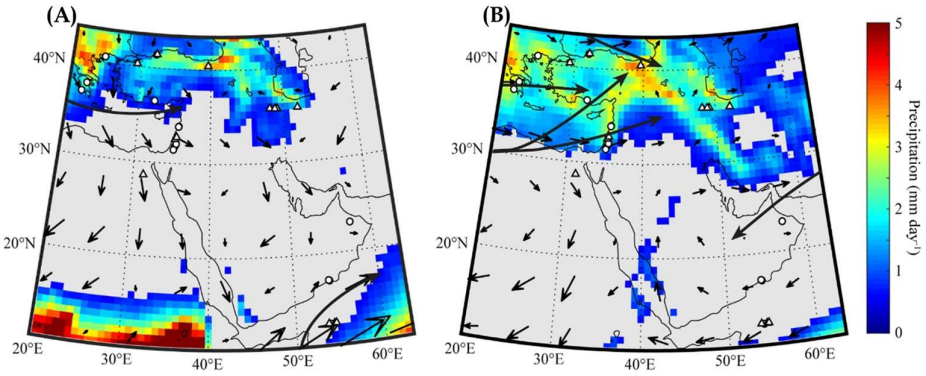

Figure 2. Maps showing seasonal precipitation amounts: (**A**) from June to September; (**B**) from December to March, together with and the 850 hPa wind fields in the Eastern Mediterranean and the Arabian Peninsula and the FC calculated from the ERA-Interim reanalysis dataset1 (1979 to 2015 CE). Grey areas indicate regions where the daily precipitation amount is smaller than 0.5 mm. Following Figure 1, circles show the location of speleothem records that are included in SISAL_v1, while triangles mark identified sites. Common trajectories of storms are superimposed on the image, show by black arrows.

Due to the high SST and low atmospheric moisture above the Mediterranean, the ratio of oxygen to deuterium isotopes yields a unique regional water line, the Mediterranean Meteoric Water Line (MMWL, $\delta D_P = 8 \times \delta^{18}O_P + \sim 22$ [‰VSMOW], [88]). As Atlantic storms traverse the Mediterranean they are imprinted with the MMWL signal, this results in the majority of EM precipitation indicating a local vapor source, rather than showing the Atlantic/Global Water Line source [88–91]. Precipitation at the southern tip of the AP and the southern parts of the Mediterranean is associated with the annual migration of the ITCZ and tropical cyclones (Figure 2), which are isotopically enriched compared to the $\delta^{18}O$ of the Atlantic/Mediterranean systems and fall closer to the Global Meteoric Water Line ($\delta D_P = 8 \times \delta^{18}O_P + 10$, [92]). Therefore, we would expect that speleothem (carbonate) $\delta^{18}O_{cc}$ time-series from the EM and the FC have different absolute values compared to the speleothem $\delta^{18}O_{cc}$ time-series from the southern tip of the AP. If, however, changes in atmospheric features (storm tracks, ITCZ) and associated precipitation changes occurred simultaneously in the EM/FC and the AP, variations in speleothem $\delta^{18}O_{cc}$ time-series should be synchronized (see Section 4.1. for details).

3. Spatial/temporal setting of Middle East speleothems

We define the ME roughly from 10ºN to 45ºN, 20ºE to 65ºE. This includes parts of Eastern Europe that are relevant for understanding the ME climate, as described in section 2. We use records from 16 caves and 23 individual speleothems from SISAL_v1 (Table 1), of which 10 sites and 17 entities are from the ME and highlighted in Figure 1. There are additional entities that are not in the SISAL_v1 database (Table 1) including sites in Turkey, Israel, Egypt, Yemen, Iran and Iraq. All $\delta^{18}O_{cc}$ values are reported in ‰ (per mille) and corrected to the Vienna Pee Dee Belemnite (VPDB) standard.

The geographic coverage of sites is uneven, with the majority of sites and entities from the EM, and a smaller proportion from the AP and FC. The geographical distribution of sites is directly linked to the spatial distribution of carbonate outcrops (Figure 1). However, other factors also have an influence. First, much of the region is arid to hyper arid (Figure 2), which inhibits the formation of speleothems, or limits formation to pluvial periods only [6,93]. Second, the recent unstable geopolitical situation in parts of the ME has allowed for limited scientific exploration.

Preprints (www.preprints.org) | NOT PEER-REVIEWED | Posted: 6 February 2019 doi:10.20944/preprints201902.0063.v1

Peer-reviewed version available at Quaternary 2019, 2, 16; doi:10.3390/quat2020016

The time intervals covered by the SISAL_v1 entities in the ME range from 0.056 ka BP (Sofular Cave) to 193 ka BP (Kanaan Cave). The temporal distribution of samples is skewed towards the Holocene, with an almost linear increase in $\delta^{18}O$ data in SISAL_v1 from ~40 ka BP to the present (Figure 3B). Only six entities extend to and beyond the last interglacial (south to north): Jerusalem West Cave AF-12, Ma'ale Efrayim ME-12, Kanaan Cave MIS5 and MIS6, Dim Cave E3 and Sofular SO-1 (Figure 3C). The remaining 17 entities are largely confined to the interval between the Last Glacial Maximum (LGM, ~22 ka BP) and present day (Table 1). The skewed distribution may be the result of publication bias, as most studies have focused on the link between climate and human civilizations [14,94], or may be a result of sporadic collection of samples from the cave sites. This suggestion is supported by the fact that large parts of the Late Pleistocene have been obtained specifically in sites where long-term continuous research has been carried out over multiple overlapping entities (e.g. Israel, Lebanon and Oman).

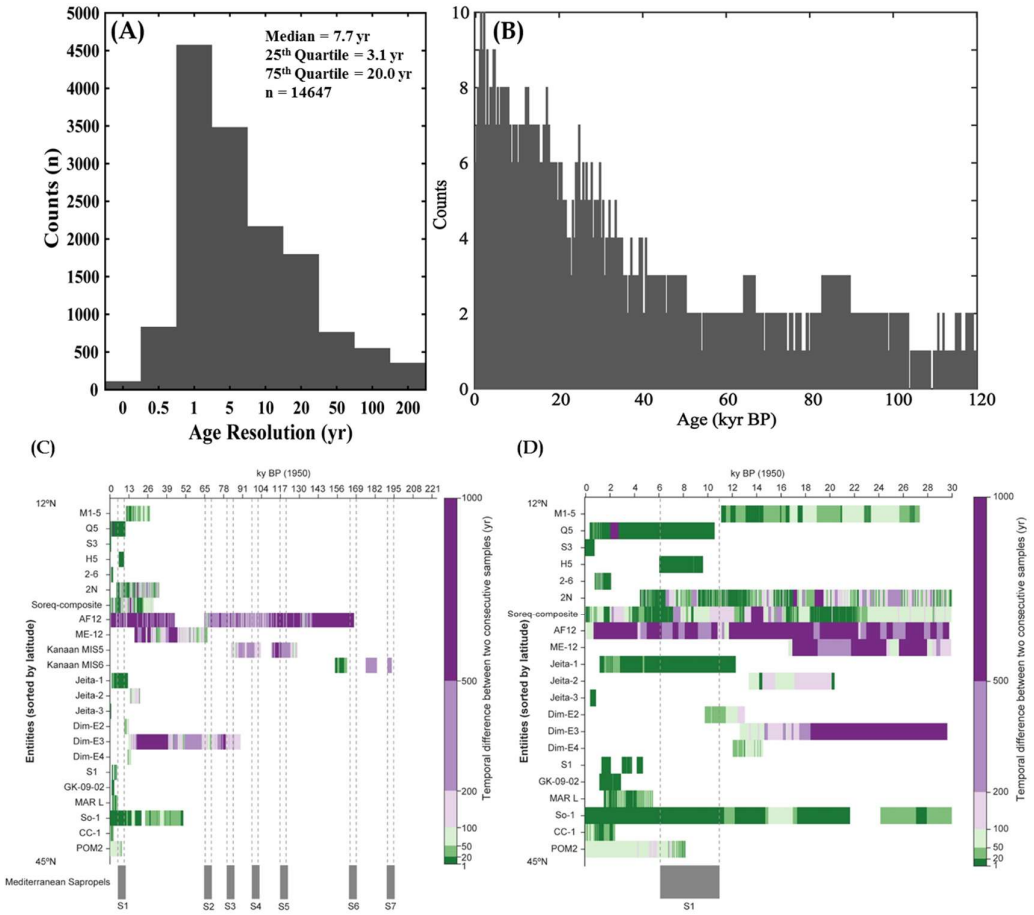

Figure 3. (A) Histogram showing the distribution of temporal difference between two consecutive data points for all ME SISAL_v1 entities, in bins of under a year (<1) to > 200 yr. **(B)** Histogram of speleothem isotope time-series of the same data set during the last 120 kyr subdivided in 250-year long bins and available speleothem isotope time-series were counted if at least one $\delta^{18}O$ value was within a bin [95]. **(C)** Temporal coverage and temporal difference of Mediterranean entities from SISAL_v1 covering the pre-Holocene time periods (up to 200 kyr) and **(D)** entities from the last 30 ka BP.

The temporal resolution of all ME samples is close to decadal (median of 7.7 year temporal gap between data points), the distribution of temporal gaps for all existing entities varies between sub-annual to >200 yr gaps (Figure 3A). Temporal resolution for all entities is given in Figures 3C and 3D (up to 100 yr gaps), showing that most entities maintain a relatively constant growth-rate, with the exception of entities from EM caves (Soreq, Ma'ale Efrayim, Kanaan Jeita and Dim sites).

This highlights the hydrological sensitivity of EM records from these regions to changes in storm tracks, rainfall amount and evapotranspiration [25,43,96].

The spatial distribution of the SISAL_v1 entities, a cross-section extending from the Balkans to the AP (Figure 1), as well as the temporal distribution and resolution, respectively, will limit the focus of our discussion to the last 30 kyr, and the regional composite to the last 12 kyr, from the Younger Dryas (YD) to present day. The temporal potential of analysis is, in most entities, limited to decadal perturbations. However, the additional entities reported in Table 1 should allow for regional compilations and coherence tests to extend beyond the late-Pleistocene and Holocene to the last inter-glacial and beyond. Moreover, the current dataset is mainly affected by Mediterranean storm tracks, with little information on the Indian Summer Monsoon (ISM). However, with the inclusion of the FC entities and the Negev Caves (Table 1) it should be easier to address questions concerning the Siberian High and ISM, not having to rely on localized data but inter-comparison between Eastern Europe and the Balkans, EM, FC and AP. For this reason, we limit this review to the last glacial period and Holocene, and in section 5 we provide suggestions to achieve a complete regional coherence analysis for the late Pleistocene.

4. SISAL_v1 entities: Site-Specific Trends and Regional Interpretation

While variations of speleothem $\delta^{18}O$ values ($\delta^{18}Occ$) are a response to changes in climate parameters (rainfall amount and distribution, storm tracks, temperature, evaporation etc.), the absolute value of precipitation $\delta^{18}O$ values ($\delta^{18}Op$) can vary between different sites, even if they respond to similar regional climate trends. As a result, the absolute value of $\delta^{18}Occ$ from different sites may not be identical (despite close to isotope equilibrium deposition). Hence, we focus on trends and excursions (i.e. on the variability) rather than absolute $\delta^{18}Occ$ values.

4.1. Controls on speleothem $\delta^{18}Occ$

The EM is optimal for isotopic studies as rainfall is limited to winter cold fronts, so there is no seasonality in precipitation or significant evaporation at the base of the cloud or after infiltration into the epikarst and karst reservoirs, respectively [90,97]. For the EM local precipitation (amount and $\delta^{18}Op$) and modern cave water have been sampled in only three of the six sites in SISAL_v1 (Kanaan, Soreq and Ma'ale Efraim). Two other sites (Mitzpe Shlagim and Pequiin) have had cave water sampled sporadically, when access to those sites was granted. Rainfall amount and isotopic compositions from the Israeli coastal plains and mountains display strong empirical correlations between rainfall amount, site altitude, and distance from the sea: all three are the underlying parameters controlling the rainout-distillation process (Rayleigh distillation) of the cloud. There is no similar correlation for desert sites as desert rainfall is affected by evaporation at the base of the cloud [90].

The most extensive monitoring project for the region was conducted in Soreq Cave between 1989 and 2016. The monitoring included the logging of rainfall amount as well as the sampling of rainfall and analyses of its composition, sampling of local ground water and host rock, cave pCO_2, relative humidity and temperature of the cave air, seasonal cave drip and pool water in multiple sites and the collection of modern speleothems and calcites [89,96–100]. The modern data from Soreq Cave reveals that on an annual time scale the "amount effect" is linearly correlated with more negative cumulative annual precipitation $\delta^{18}Op$, and that this trend is then transferred into the cave, resulting in wetter years displaying more negative winter cave water $\delta^{18}O$ ($\delta^{18}Ocw$), while droughts shift the baseline seepage drip to more positive $\delta^{18}Ocw$ values [98]. The decadal to seasonal variations were validated in a modern stalagmite sample [96] and also observed in Soreq Cave fossil speleothem records, in seasonal to centennial resolution [14,24,27].

4.2. The Last Glacial Maximum, deglaciation and the transition into the Holocene (30 kyr BP to Holocene)

Although precipitation amount may be the driver of Holocene variations, EM records for the glacial-inter-glacial transition of the late Pleistocene (deglaciation), follow the Mediterranean

planktonic curves, indicating that the EM speleothems $\delta^{18}O$ record primarily reflects sea surface $\delta^{18}O$ changes [50,65,101,102]. Large glacial positive $\delta^{18}Occ$ shifts are expected as a result of the changing $\delta^{18}Occ$ composition of the source, i.e. the Mediterranean Sea ("source effect"). This shift is most pronounced in Soreq Cave, where a sharp decrease in $\delta^{18}Occ$ is visible starting at the Last Glacial Maximum (LGM) from -3 ‰ towards Holocene values of -5.5 ‰ (Fig 4). The depletion trend stabilizes at about 15ky BP (Greenland warm Interstadial, GI1, or Dansgaard-Oeschger D/O events), followed by a pronounced response to the Younger Dryas (YD), the strongest observed in the SISAL_v1 records from the region, with an enrichment of > +1.5‰. The Soreq composite record also records global events in the period out of the last glacial, e.g GI-4, 3 and 2 as well as Heinrich event 1 (H1) and the YD (Figure 4).

The Jeita, Ma'ale Efrayim and Jerusalem West entities all have lower temporal resolution during the LGM and deglaciation which makes the identification of major climatic events difficult in their time-series (Figure 4). On centennial and higher time-scale, we observe in these records a more gradual transition in the $\delta^{18}Occ$ values, starting only after the LGM (circa ~17.5 ka BP) from -2.5 ‰ towards Holocene depleted $\delta^{18}Occ$ values ranging between -~ -5 and -7 ‰ in Dim, Jeita and West Jerusalem caves (Figure 4). The expected "back to glacial" excursion of the YD is most prominent in the Soreq composite record (~ +1‰), and is harder to identify in neighboring Levant records in SISAL_v1 (Fig 4). The identical trends observed across EM records suggest that they were responding to the same regional climatic drivers, specifically, changing storm tracks, encroaching coastlines and change in EM sea surface isotopic composition [48,49,77,90]. This can be seen in Jeita Cave, which displays a first order correlation with EM marine foraminifera $\delta^{18}O$ (i.e. SST and composition) and to the EM speleothem $\delta^{18}Occ$ trend observed in the composite time-series of the Levant (Figure 6G). However, during prominent climatic events (LGM, H1) entity Jeita-2 $\delta^{18}Oc$ time-series shows opposite trends to the marine records [103,104], these excursions towards lighter $\delta^{18}Occ$ are often in tandem with lower $\delta^{13}Ccc$ and Sr/Ca values, associated with a high precipitation to evaporation ratio (i.e. higher potential rainfall infiltration). Evidence of changes in palaeo-infiltration variations highlight the inconsistencies between the climates deduced from the marine record vs. that from terrestrial, and that the source effect, is not the only parameter influencing variations in $\delta^{18}Occ$.

Sofular Cave entity SO-1, however, is the only time-series which does not agree with this glacial to inter-glacial regional trend, gradually shifting towards more isotopically enriched values in the transition to the Holocene (Figure 4). The distinct imprint of Greenland interstadials on the MIS2 50-kyr record suggests that SO-1 records decadal to centennial-scale events, however, on glacial time-scales the $\delta^{18}Occ$ records Black Sea surface water composition rather than Mediterranean source which determines most of the EM coastline records [56]. Additional discussion on Sofular cave, including the Holocene cycle documented in the speleothem $\delta^{13}C$ time-series, can be found in the review of Eastern European records in SISAL_v1 [37].

The majority of entities from the AP grew only in interglacial periods. The only entity growing from the LGM to the Holocene is M1-5, Moomi Cave (Socotra Island), from 27 ka to 11 ka BP. The north-easterly autumn rains are the main source of infiltrating water for Moomi Cave and are sourced from the ITCZ. Most of the Moomi $\delta^{18}Occ$ record is strongly correlated with the Greenland ice cores, suggesting a possible Atlantic driver of these monsoonal shifts [54]. Thus, sample M1-5 records late Pleistocene global climatic events. The LGM is dated in the record as occurring circa 23 ka BP and marked by aridification and decrease in precipitation over the Island, followed by an increase in rainfall from LGM, interpreted from a $\delta^{18}Occ$ depletion trend similar but more gradual than seen in the Soreq record, to the H1 event (~16.4 ka BP warm/dry event), followed by the Bølling-Allerød (14.5 ka wet event) and the dry YD. The entity terminates soon after the commencement of the Holocene (dated to 11.4 ka), marked by a sharp decrease in $\delta^{18}Occ$ value which is interpreted as increase in monsoonal rainfall. The Levant records (Soreq, Jerusalem west and Ma'ale Efrayim) do not show a concomitant abrupt change of ~30 years transition from YD to Holocene.

Preprints (www.preprints.org) | NOT PEER-REVIEWED | Posted: 6 February 2019 doi:10.20944/preprints201902.0063.v1

Peer-reviewed version available at Quaternary 2019, 2, 16; doi:10.3390/quat2020016

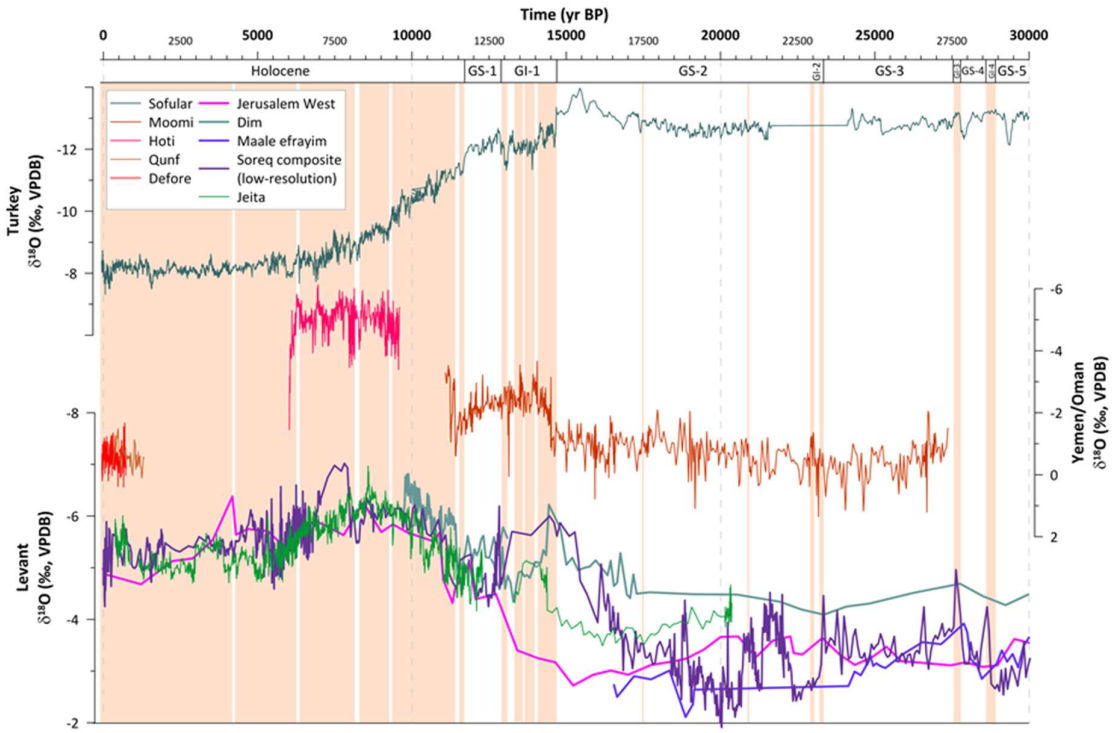

Figure 4. Time-series of δ^{18}Occ of speleothem records from the AP (Yeman/Oman), EM (Levant including Turkeys' Mediterranean coast, i.e., Dim Cave) and Northern Turkey (Sofular). The climatic events highlighted on the plot (and expended in Figures 5A and 5B) are based on the interpretations from references [26,105,106]

4.3. Holocene climatic events and spatial heterogeneity across the Middle East

The Holocene is characterized by a general trend towards increasing aridity in the ME region [44,46,56,61,65,107–109]. The wettest period in the Eastern Mediterranean, and the Levant in particular, occurred from about 10 to 7 ka BP, coeval to the formation of Mediterranean sapropel 1 [63,110,111]. The entity from Jeita cave (Figure 5A), shows increasing precipitation during the early Holocene (from 12 to 10 ka BP) and wet conditions between 10 to 7 ka BP with peak precipitation at about 8.5 ka BP. Between 7.5 and 6.5 ka BP the δ^{18}Occ time-series from Jeita cave indicates a general decreasing trend in precipitation amounts until 5 ka BP. Then precipitation amounts are nearly similar to pre-Holocene levels, at about 12 ka BP. The late Holocene in this entity is characterized by generally dry conditions with shorter and longer wet-periods, e.g. from 4.0 to 3.0 ka BP, when precipitation amounts were increased. The hydroclimate changes recorded at Jeita cave are in general agreement with other speleothem δ^{18}Occ time-series from the region, such as with the speleothem records from Soreq Cave (Israel) [59] and Dim Cave (Turkey) [45] (Figure 5A). All these records indicate that the most arid conditions in the Holocene occur after ~3.2 ka BP [49,53].

The only other record from the EM that spans the entire Holocene is entity SO-1 from Sofular cave (Figure 5A). This record shows increasing δ^{18}Occ values during the early- and mid-Holocene, until about 6 ka BP. However, compared to other records from the Eastern Mediterranean, long-term δ^{18}Occ trends in SO-1 are not related to variations in precipitation amounts, but reflects changes in the mean δ^{18}O value of the Black Sea [56,57]. Therefore, it is not possible to link long-term δ^{18}Occ changes from SO-1 to the long-term δ^{18}Occ changes from the Eastern Mediterranean speleothems. A speleothem record from Eastern Europe, Ascunsa Cave (Romania), shows similar long-term changes as SO-1 (Figure 5A), which likely reflects also δ^{18}O changes of the Black Sea, though the main source of vapor for this cave are central Mediterranean cyclones, possibly the result of terrestrial moisture recycling [108].

A well-documented archaeological history of the Near East is available over the Holocene [112] (Figure 6A), coeval with the growth period of many of the Middle Eastern entities (Figure 3). We compile a composite of ME speleothem datasets from the past 11 kyr (Figure 6G). Record compilations have yielded useful results in the study of the past 2000 years [38,39,113] in that it mitigates the effect of age uncertainties and enables a uniform focus on detectable climate variability. Here the composite was produced as follows: first, data from each of the reconstructions were averaged into bins (at 25-year and 200-year intervals); second, each binned series was then standardized by its average and standard deviation. The standardized anomalies are visualized as boxes [width: 200-year intervals; central mark: median; edges of the box: 25th to 75th percentile range; whiskers: extreme values (~99% of data); plusses: outliers (~1% of data)] connected with a 3-point running average of the 25-year bin means (Figure 6G). For comparison, the same process is applied to publicly available records such as Greenland ice cores [114] and Mediterranean marine archives covering the Holocene [115,116] (Figure 6D, H).

Rapid, prominent events, observed in both continental and marine palaeo-archives during glacial periods, are evident, albeit less pronounced, during the Holocene. The presence/absence of the ice sheets is a significant change between variable ice-ages and stable warm periods; ice sheets are enormous mountain ranges of high albedo, which necessarily create a huge orographic feature during a glacial and concomitant shifts in wind patterns [117]. This persistent rapid variability could be the response to an internal rhythmic throbbing of the climatic system at centennial scales, manifested independently of the glacial and interglacial cycles, but less obvious in the geological record when large ice sheets are absent [118]. The repetitive pattern of observed oscillations does not imply periodicity [119,120]. Indeed, the study of the sum of cold periods and dry phases over the Holocene [28] point to a variety of non-periodic events, each one with its particularities (Figure 6F,I). In the scope of this review, three Holocene events are reviewed: ca. 8200 years BP (referred to here as the 8.2k event), ca. 4200 years BP (4.2k event) and ca. 700 years BP (0.7k or the Little Ice Age, LIA), which are those recorded coeval with major glacier advances in the northern hemisphere [28](Figure 6E).

The base of the Holocene is defined in the North Greenland Ice Core Project's NGRIP2 ice core, at 11650 years BP [121]. The Early/Lower Holocene goes from the base to the 8.2k event [122]. The 8.2k event seems coeval with a final drainage of northern ice-dammed lakes causing a freshwater outburst into the North Atlantic [123]. Pronounced cold temperatures lasting ca. 160 years are recorded in Greenland, together with a general decrease snow-accumulation rate [124]. It is an outstanding event in the context of the rest of the Holocene, which is characterized by a gradual cooling trend [114]. The event is preceded by a remarkable minimum in solar activity [125] and an increase in the magnitude and frequency of volcanic eruptions characterizing the final stages of the deglaciation [126] (Figure 6B). The Dead Sea level was sustained at low with a very subdued level rise during the 8.2k event, which would suggest anomalously rainfall intensities (Figure 6C).

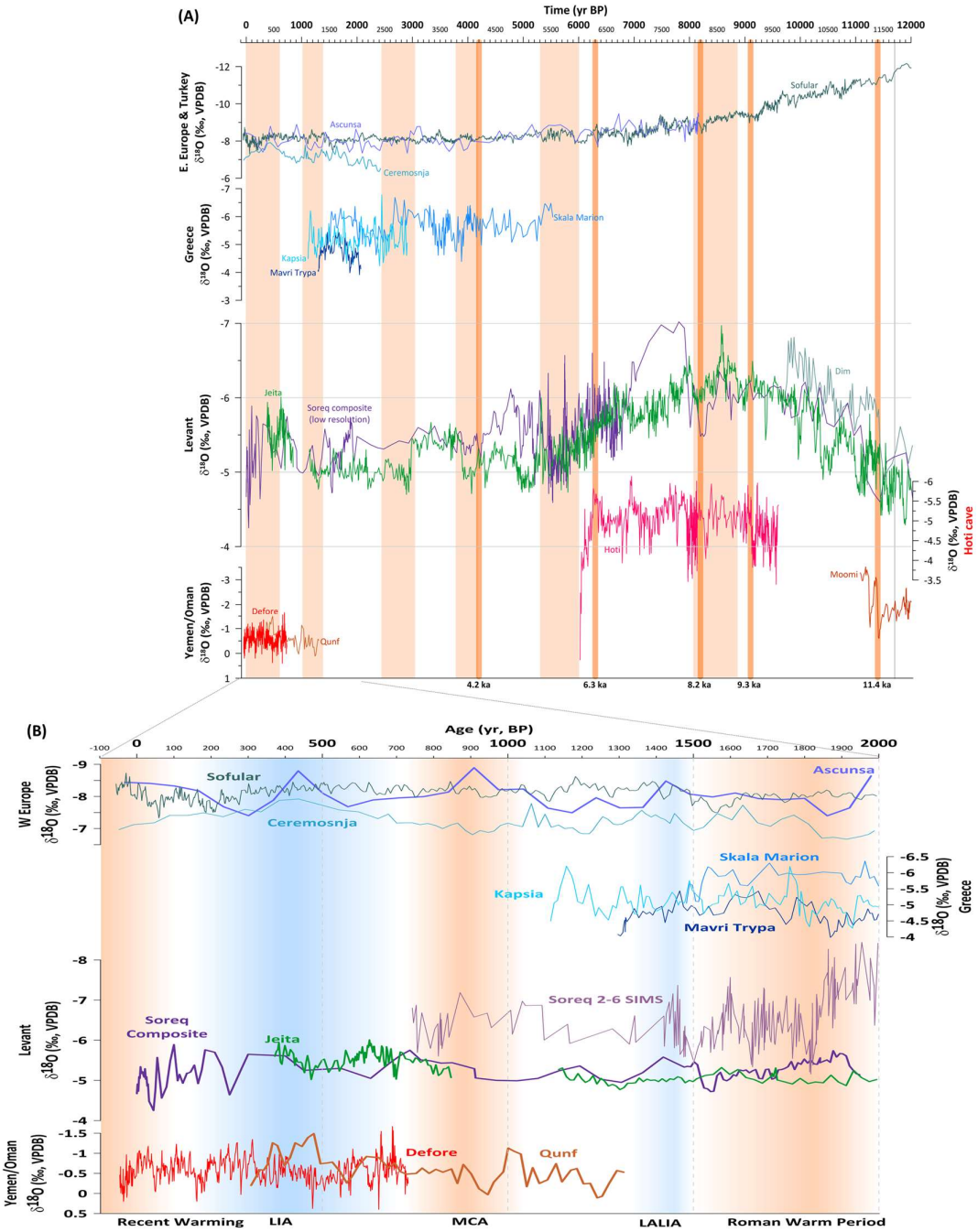

Figure 5. (A) Time-series of δ^{18}Occ of speleothem records from Figure 4, only for the last 12 kyr. This figure includes two entities from Eastern Europe (Ceremosnja and Ascunsa, see Table 1 for details) compared against Sofular Cave (SO-1), and three entities from Greece (Kapsia, Skala Marion and Marvi Trypa Caves). These caves are on the modern dominant storm trace to the ME region (Figure 2). **(B)** Similar records to Figure 5A for the last 2 kyr. Added for discussion is the 5 µm-high-resolution spatial analysis of Soreq Cave entity 2-6 [14]. The climatic events highlighted on the plot are based on the interpretations from references [26,105,106]

The majority of the ME entities trace the 8.2k event as a positive anomaly, within the generally humid period associated to the last sapropel (Figure 6F-G). Sapropels are recorded in marine sediments due to a change either in the flux of organic matter to the sea floor from productivity changes or in preservation by bottom-water oxygen levels [127,128]. Factors such as monsoon intensification, increased runoff from North Africa into the Mediterranean Sea and preconditioning due to meltwater events/sea-level rise are potential factors leading to sapropels [129,130]. The particular geomorphology and hydrology of the Mediterranean basin favours their deposition, together with the known African Humid period, with a wet and vegetated Sahara [127,131,132]. The 8.2k event would appear in the SISAL ME compilation as an interruption of this generally humid period (Figure 6G). Marine sediments record the event as a cold reversal consistent with the North Atlantic context [28,115,116] (Figure 6H, I). In the Levant, the 8.2k event might be coeval with Neolithic revolution traits (e.g. the transition from Pre-Pottery to Pottery periods) [112] (Figure 6A). However, in the western basin of the Mediterranean, the 8.2k event could be closely related to an archaeological "silence" in one of the main Iberian river basins [133] and a Mesolithic techno-typological transition [134].

There is a variety of signals in the entities of SISAL_v1 for the 4.2k event: Jeita Cave (Figure 5A) indicates that precipitation increased at the northern Levantine coast, while the Soreq δ^{18}Occ time-series points to a precipitation decrease. However, if compared to the δ^{18}Occ time-series from Jeita Cave, and when considering the age and proxy uncertainties of the Soreq composite time-series, it is also reasonable to argue that the precipitation increase right after the 4.2 ka event is too young and should be at 4.2 ka BP. The only other entity which covers the 4.2 ka event is the δ^{18}Occ time-series from Skala Marion, Greece (Figure 5A) and reflects rather stable climatic conditions. In this regard, integration of all the previous ME speleothems signals would suggest a 4.2k event as the culmination of a gradual increase in aridity (Figure 6G). The event was preceded by advance of glaciers in the northern hemisphere [28] and a Dead sea level drop lasting for about five centuries [135] (Figure 6C-E). The 4.2k event could be associated with the end of the African Humid Period, which was apparently time-transgressive; i.e. progressed from north to south, following a gradual reduction in monsoon rainfall, due to the southward migration of the tropical rain belt [136,137]. Nevertheless, North African human settlements appear to have been abandoned in less than a millennium (ca. from 6300 to 5200 years ago), which suggests local environmental conditions and societal activities, can respond nonlinearly to climate change [132,138,139]. Cultural changes and settlement abandonment are seen from the Near East to northern Mesopotamia as part of the end-phases of the Bronze age [112,140] (Figure 6A).

For the last 2 kyr, entities from Sofular Cave, Kapsia Cave, Mavri Trypa, Soreq Cave, Jeita Cave, Qunf Cave and Defore Cave are available (Figure 5B). From these records only SO-1 from Sofular Cave covers the entire period at a relatively high temporal resolution. The largest variability is observed in sample Soreq 2-6 SIMS, which was generated using Secondary Ion Mass Spectrometry (SIMS) [14,66]. Interestingly the absolute value of the SIMS δ^{18}Occ has more negative values compared to the δ^{18}Occ of the Soreq composite record and a much larger δ^{18}Occ variability. This is possibly related to the SIMS-sampling methodology which targets multiple analyses in a single ~50-100µm thick annual band, thus emphasizing the -2.15‰ lighter winter values [14]. The Soreq 2-6 δ^{18}Occ indicates a drying trend from 2 to 1.8 ka BP that is not observed in the other δ^{18}Occ time-series from the Eastern Mediterranean (Figure 5B); instead the mean δ^{18}Occ of these time-series is more or less constant. This is possibly also provoked by the relatively low temporal resolution of these records, allowing to resolve only pronounced changes in δ^{18}Occ. The finer climate variations during the Medieval Climate Anomaly (MCA) and the Late Antique Little Ice Age (LALIA) [106] are identifiable only in Soreq 2-6. The Little Ice Age (LIA) is recorded by the Levantine Coast entities (mainly Jeita Cave) and the record from Defore Cave (Figure 5B).

The comparison between the AP and the EM over the past 2000 years is limited by the overlap of the entities available. The transition from the LALIA to the MCA is characterized by variable δ^{18}Occ values in Soreq 2-6. At the beginning of the LALIA δ^{18}Occ values are negative in Soreq 2-6 indicating a generally wet conditions in the southern Levant (consistent with the Soreq composite

record), while at the end of the LALIA δ^{18}Occ values are more positive indicating dryer conditions during the period from the LALIA to the MCA. At the MCA precipitation amounts increased again in the EM, indicated by the negative trend in δ^{18}Occ values in Soreq 2-6 [14,48,141]. During the MCA, δ^{18}Occ changes in the Qunf record and in Soreq 2-6 are anti-correlated, suggesting opposite precipitation variations at the southern tip of the AP and in the EM. For the LIA at 0.7 ka BP that lasts for about 100 years, when δ^{18}Occ values begin to decrease again, while the speleothem from Jeita Cave stops to grow at 0.4 ka BP the δ^{18}Occ time-series from Defore Cave covers the entire LIA, and opposite patterns between both regions cannot be excluded. It reveals that apart from the aforementioned dry-wet alternation no large changes in the mean δ^{18}Occ values are observed. This would be consistent with the (low-resolution) δ^{18}Occ Soreq composite (Figure 5B). Therefore, it appears that for the last 1.5 kyr only during the MCA precipitation changes in the EM and southern Arabia were anti-correlated.

The ME composite allows detectable changes to be investigated, even when regarding the resolution issues in some of the included entities. The LIA is the latest anomaly of the Late/Upper Holocene and had strong impacts on European societies [142,143]. Greenland ice cores show the coldest individual bins of the past 2000 years during this period (Figure 6D). The ME speleothems show extreme variability established after the 4.2k event, though around what seem to be coldest periods in the North Atlantic [28], show a tendency towards more moisture available, consistent with Dead sea level spells (Figure 6C,G,I). The more dispersed bins in marine sediments are observed for the past 2800 years, and the 0.7ka is the last cold reversal recorded, more severe in its late phase (Figure 6H). Forcing simulations suggest that this pattern is consistent with a global cooling trend, which arises from increased frequency of volcanism and/or land use change [38] (Figure 6B). Studies in the North Atlantic show several phases and year-to-year variability during the Little Ice Age: severe droughts, floods, intense storm activity during late summer-early autumn, cold/heat waves that showed significant spatio-temporal variation and exceptional wintertime conditions, with sea ice expansion and reduced northward heat transport by the subpolar gyre [144–146]. In the Levant, the onset of the Little Ice Age coincides with the end of the Crusades and reinforcement of the Mamluk sultanate and Ottoman empire over much of Southeast Europe, Western Asia and North Africa between the 14th and early 20th centuries [112] (Figure 6A).

5. Conclusions and Future of SISAL project in the Middle East

5.1. Emphasis for future speleothem research in the Middle East

The main goal for future speleothem research in the ME would be to increase spatial coverage in the region (Figure 1, Table 1 – identified entities), specifically in the water limited FC, AP regions and Saharan belt (Egypt, Negev). Additionally, emphasis should be placed on high temporal-resolution analysis (applying conventional and novel methods) to increase the temporal coverage of the geological past (Figure 3) and allow detection of changes in seasonality [14,27] and decadal scale variations [24,43].

The first goal is important to better constrain teleconnections between the hydroclimate of remote regions such as Northern Africa, the EM and the FC, which should all be influenced by Mediterranean cyclones and ITCZ migration. Furthermore, considering the location of the EM at the border between the tropical Hadley cell and the mid-latitude Ferrel cell, hydroclimate changes in these regions are supposed to be very sensitive to shifts in the Hadley-Ferrel-cell border, which should be ultimately imprinted in the speleothem palaeoclimate record. Hence, future speleothem-based reconstructions and synthesis of past hydroclimate changes from North Africa, the Levant and the FC will allow testing of theoretical concepts on how the Hadley-Ferrel-cell border should shift in response to changes in insolation [147].

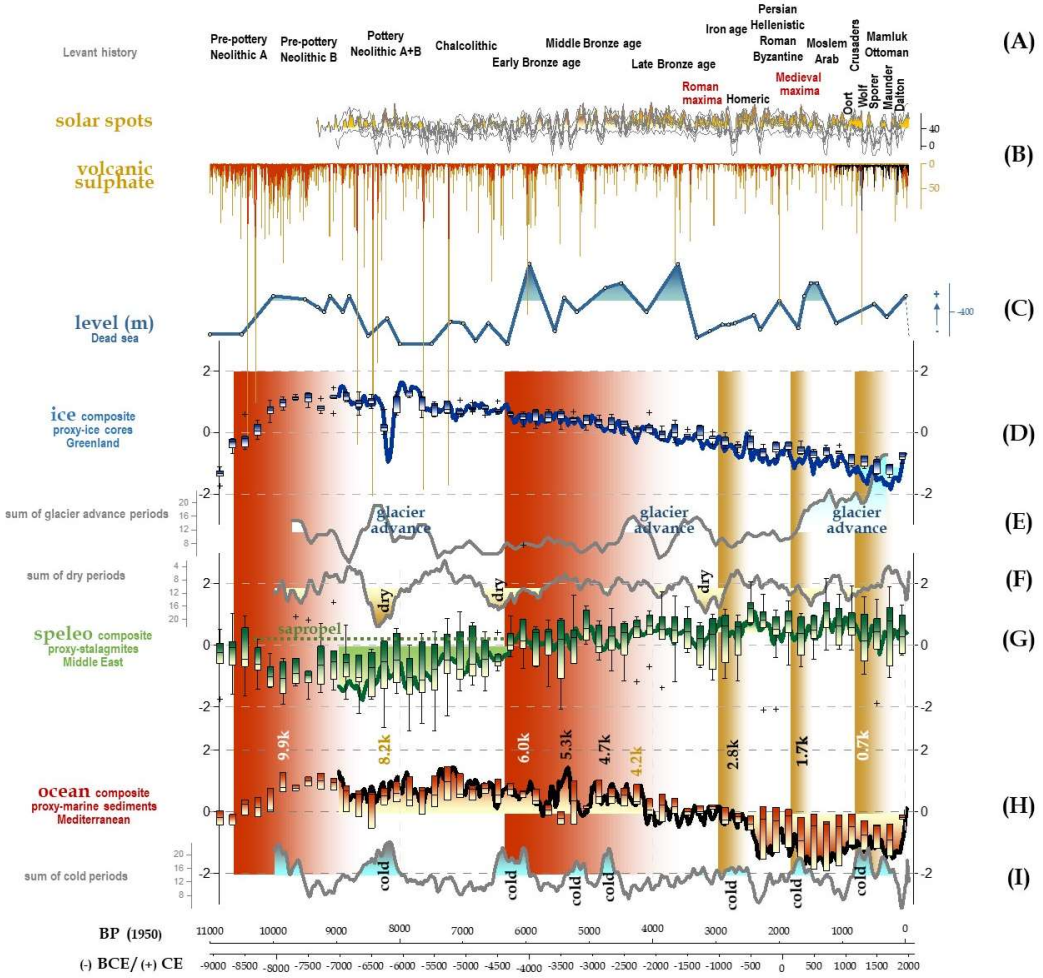

Figure 6. Holocene overview of the δ^{18}Occ of ME speleothem records in comparison with additional terrestrial and marine palaeo-archives. **(A)** Historical-archaeological phases in the Levant [112]. **(B)** Reconstructed sunspot number along with its 68% confidence interval [125] and volcanic aerosol based on empirical orthogonal function analysis performed in ice cores from Greenland [126,148]. **(C)** Dead sea level changes [135]. **(D)** Composite the δ^{18}O from Greenland ice-cores [114].**(E, F)** Sum of ice glacier advances and dry periods [28]. **(G)** Composite of the SISAL δ^{18}Occ from ME and Eastern Europe speleothems reviewed in the previous section [32]. **(H)** Composite of Mediterranean Sea surface temperatures covering the Holocene [115,116]. Composites are shown as standardized anomalies (standard units) [box width: 200-year intervals; central mark: median; edges of the box: 25th & 75th percentiles; whiskers: extreme values (~99% of data); plusses: outliers (~1% of data); boxes connected with a 3-point running average of 25-year bin means]. **(I)** Sum of cold periods [28].

It is also important to generate longer time-series from the region as most of the records cover only the last 40-30 kyr (Figure 2B). This will enable future studies to conduct more accurate coherence regional investigations to reveal climate mechanisms over longer time periods, including glacial-inter-glacial cycles in the Pleistocene.

The ability to simulate the rhythm of climate variability and specific events (such as sapropels, the 8.2k or 4.2k events, the LIA and the like) will depend on the availability of high quality databases, with sufficient temporal resolution to make relevant inferences from a human perspective. In this regard, completion of the above mentioned information will help in answering challenging questions and in understanding changes to come in water limited environments.

5.2. The importance of Fertile Crescent speleothem data

The publication of more speleothem-based proxy records from the FC is a priority in palaeoclimatic research for several reasons. Firstly, additional FC entities would make it easier to establish the role of the Siberian High and ISM in the regional palaeo-hydrology. Whereas there is no influence from the summer monsoon on precipitation in the modern-day FC, it has been theorized that in the early Holocene (and before) the picture was more complicated – the FC received rainfall more evenly from two sources instead of the simple single-source nature of precipitation today [149].

Additionally, late Holocene δ^{18}Occ records from the FC, and elsewhere in the ME, reflect winter-spring precipitation amount, the main hydrological season. Other records (lake sediments, tree-rings) from the region often reflect annual precipitation, summer precipitation or temperature changes. They can also suffer from other inadequacies such as lacking the required temporal resolution, not covering the researched period, or suffering from considerable chronological uncertainties [149]. These problems are especially limiting when using palaeoclimate proxies in archaeological discussions, as tying climatic events to specific human developments requires maximum chronological precision and precipitation during the growing period (spring) will be most important for human flourishing. Seeing as the FC is perhaps the most important region worldwide for human development, producing highly-resolved and accurately-dated speleothem records is of vital concern. Here we identified five sites in the FC, from Turkey, Iran and Iraq. The entities from these publications have already contributed to the understanding of the prevailing continental climatic conditions over the Holocene and as far back as 500 ka BP. Augmenting the available datasets and future studies in to the SISAL database would provide an important tool for answering the questions raised in this section.

5.3. SISAL outlook for the Middle East

As Table 1 suggests, there is an excellent opportunity to include more records from the ME in the SISAL database. This would allow the application of sophisticated statistical analyses, e.g. standardization techniques to synthesize common trends in the stable isotope time-series [38] or Monte Carlo Principal Component Analyses (MC-PCA) [31]. Such analyses will allow better constraints on the relationships between different archives such as between the speleothem hydroclimate record from the ME and reconstructed SSTs. It would also allow the identification of common modes of hydroclimate variability and a better understanding of the climate dynamics/mechanism and its forcing. Coherence analyses (e.g. MC-PCA) should be extended by including Western Mediterranean as well as European stable isotope time-series, respectively, to validate the teleconnection between hydroclimate changes that also depend on mid-latitude cyclones [150–152].

Supplementary Materials: Figure S1: Entity-specific spatial and temporal distribution.

Author Contributions: YB designed the concept of this study and led the writing of this manuscript with support of all co-authors. MD assisted in data extraction from the SISAL_v1 software, original draft preparation and statistical analysis as well as assistance in design of Figure 2 and 3. MAL and EIA did most of the visualization work of Figure 4. BM and JFL worked on the draft preparation and statistical analysis to lead to Figure 6.

Funding: MD acknowledges funding by the German Research Foundation (DFG) grant DE 2398/3-1. MAL acknowledges support from the Ministry of Science and Technology (MOST), Taiwan (107-2119-M-002-051). YB acknowledges fun. BM acknowledges support from the CSIC Ramón y Cajal postdoctoral programme RYC-2013-14073.

Acknowledgments: SISAL is a working group of the Past Global Changes (PAGES) programme and we thank PAGES for their support of this activity. We thank Laia Comas-Bru for assistance in Figure 1, and sharing the design for Figure S1. The authors thank the members of the World Karst Aquifer Mapping project for providing the carbonate aquifer maps used by Laia Comas-Bru for Figure 1. We are grateful to Sandy Harrison and Laia Comas Bru for their editorial handling of the manuscript and endless patience. YB wishes to thank Kerstin

Braun and Zoltán Kern for coordination in preparation of the African and Eastern European review papers included in this special issue [37,153], and Miryam Bar-Matthews for her support in the SISAL Middle East team efforts to advance the input of regional datasets into v1 and v2.

Conflicts of Interest: The authors declare no conflict of interest. The funders had no role in the design of the study; in the collection, analyses, or interpretation of data; in the writing of the manuscript, or in the decision to publish the results.

References

1. Katrantsiotis, C.; Kylander, M.E.; Smittenberg, R.; Yamoah, K.K.A.; Hättestrand, M.; Avramidis, P.; Strandberg, N.A.; Norström, E. Eastern Mediterranean hydroclimate reconstruction over the last 3600 years based on sedimentary n-alkanes, their carbon and hydrogen isotope composition and XRF data from the Gialova Lagoon, SW Greece. *Quat. Sci. Rev.* **2018**, *194*, 77–93.
2. Lionello, P.; Abrantes, F.; Congedi, L.; Dulac, F.; Gacic, M.; Gomis, D.; Goodess, C.; Hoff, H.; Kutiel, H.; Luterbacher, J.; et al. Introduction: Mediterranean Climate – Background Information. In *The Climate of the Mediterranean Region: From The Past to the Future*; Lionello, P., Ed.; Elsevier: London, 2012.
3. Giorgi, F. Climate change hot-spots. *Geophys. Res. Lett.* **2006**, *33*, 1–4.
4. Giorgi, F.; Lionello, P. Climate change projections for the Mediterranean region. *Glob. Planet. Change* **2008**, *63*, 90–104.
5. Lionello, P.; Scarascia, L. The relation between climate change in the Mediterranean region and global warming. *Reg. Environ. Chang.* **2018**, *18*, 1481–1493.
6. Vaks, A.; Bar-Matthews, M.; Ayalon, A.; Matthews, A.; Halicz, L.; Frumkin, A. Desert speleothems reveal climatic window for African exodus of early modern humans. *Geology* **2007**, *35*, 831.
7. Rosen, A.M. *Civilizing Climate: Social Responses to Climate Change in the Ancient Near East*; Altamira Press: Plymouth, 2007; ISBN 978-07591-0494-5.
8. Berger, J.F.; Lespez, L.; Kuzucuoğlu, C.; Glais, A.; Hourani, F.; Barra, A.; Guilaine, J. Interactions between climate change and human activities during the Early to Mid Holocene in the East Mediterranean basins. *Clim. Past* **2016**, *12*, 1847–1877.
9. Schilman, B.; Bar-Matthews, M.; Almogi-Labin, A.; Luz, B. Global climate instability reflected by Eastern Mediterranean marine records during the late Holocene. *Palaeogeogr. Palaeoclimatol. Palaeoecol.* **2001**, *176*, 157–176.
10. Langgut, D.; Almogi-Labin, A.; Bar-Matthews, M.; Pickarski, N.; Weinstein-Evron, M. Evidence for a humid interval at ~56–44 ka in the Levant and its potential link to modern humans dispersal out of Africa. *J. Hum. Evol.* **2018**, *2018*.
11. Brierley, C.; Manning, K.; Maslin, M. Did pastoralism delay the collapse of the green Sahara 6000 years ago ? **2017**, 1–23.
12. Weiss, H.; Bradley, R.S. What drives societal collapse? *Science (80-.).* **2001**, *291*, 609–610.
13. Bar-Matthews, M.; Ayalon, A. Climatic Conditions in the Eastern Mediterranean During the Last Glacial (60 – 10 ky) and Their Relations to the Upper Palaeolithic in the Levant as inferred from Oxygen and Carbon Isotope Systematics of Cave Deposits. In *More than meets the eye: studies on Upper Palaeolithic diversity in the Near East*; Goring-Morris, N.A., Belfer-Cohen, A., Eds.; Oxford: Oxbow, 2003; pp. 13–18.
14. Orland, I.J.; Bar-Matthews, M.; Kita, N.T.; Ayalon, A.; Matthews, A.; Valley, J.W. Climate deterioration in the Eastern Mediterranean as revealed by ion microprobe analysis of a speleothem that grew from 2 . 2 to 0 . 9 ka in Soreq Cave , Israel. *Quat. Res.* **2009**, *71*, 27–35.
15. Rosenberg, T.M.; Preusser, F.; Fleitmann, D.; Schwalb, A.; Penkman, K.E.H.; Schmid, T.W.; Al-Shanti,

M. a.; Kadi, K.; Matter, A. Humid periods in southern Arabia: Windows of opportunity for modern human dispersal. *Geology* **2011**, *39*, 1115–1118.

16. Fleitmann, D.; Burns, S.J.; Pekala, M.; Mangini, A.; Al-Subbary, A.A.; Al-Aowah, M.; Kramers, J.; Matter, A. Holocene and Pleistocene pluvial periods in Yemen, southern Arabia. *Quat. Sci. Rev.* **2011**, *30*, 783–787.
17. Vaks, A.; Woodhead, J.D.; Bar-Matthews, M.; Ayalon, A.; Cliff, R.A.; Zilberman, T.; Matthews, A.; Frumkin, A. Pliocene–Pleistocene climate of the northern margin of Saharan–Arabian Desert recorded in speleothems from the Negev Desert, Israel. *Earth Planet. Sci. Lett.* **2013**, *368*, 88–100.
18. Vaks, A.; Bar-Matthews, M.; Ayalon, A.; Schilman, B.; Gilmour, M.A.; Hawkesworth, C.J.; Frumkin, A.; Kaufman, A.; Matthews, A. Paleoclimate reconstruction based on the timing of speleothem growth and oxygen and carbon isotope composition in a cave located in the rain shadow in Israel. *Quat. Res.* **2003**, *59*, 182–193.
19. Weisdorf, J.L. 1. From Foraging To Farming: Explaining The Neolithic Revolution. *J. Econ. Surv.* **2005**, *19*, 561–586.
20. Tanno, K.I.; Willcox, G. How fast was wild wheat domesticated? *Science (80-.).* **2006**, *311*, 1886.
21. Zohary, D.; Hopf, M. Domestication of Pulses in the Old World: Legumes were companions of wheat and barley when agriculture began in the Near East. *Science* **1973**, *182*, 887–894.
22. Liverani, M. *The Ancient Near East: History, Society and Economy.*; Routledge: New York, 2014;
23. Mellaart, J. *The neolithic of the Near East*; Scribner's: New York, 1975; ISBN 0-684-14484-0.
24. Bar-Matthews, M.; Ayalon, A. Mid-Holocene climate variations revealed by high-resolution speleothem records from Soreq Cave, Israel and their correlation with cultural changes. *The Holocene* **2011**, *21*, 163–171.
25. Flohr, P.; Fleitmann, D.; Zorita, E.; Sadekov, A.; Cheng, H.; Bosomworth, M.; Edwards, R.L.; Matthews, W.; Matthews, R. Late Holocene droughts in the Fertile Crescent recorded in a speleothemfrom northern Iraq. *Geophys. Res. Lett.* **2017**, *44*, 1528–1536.
26. Mayewski, P.A.; Rohling, E.J.; Curt Stager, J.; Karlén, W.; Maasch, K.A.; David Meeker, L.; Meyerson, E.A.; Gasse, F.; Van Kreveld, S.; Holmgren, K.; et al. Holocene climate variability. *Quat. Res.* **2004**, *62*, 243–255.
27. Orland, I.J.; Bar-Matthews, M.; Ayalon, A.; Matthews, A.; Kozdon, R.; Ushikubo, T.; Valley, J.W. Seasonal resolution of Eastern Mediterranean climate change since 34ka from a Soreq Cave speleothem. *Geochim. Cosmochim. Acta* **2012**, *89*, 240–255.
28. Wanner, H.; Solomina, O.; Grosjean, M.; Ritz, S.P.; Jetel, M. Structure and origin of Holocene cold events. *Quat. Sci. Rev.* **2011**, *30*, 3109–3123.
29. Kelley, C.P.; Mohtadi, S.; Cane, M.A.; Seager, R.; Kushnir, Y. Climate change in the Fertile Crescent and implications of the recent Syrian drought. *Proc. Natl. Acad. Sci.* **2015**, *112*, 3241–3246.
30. Trigo, R.M.; Gouveia, C.M.; Barriopedro, D. The intense 2007-2009 drought in the Fertile Crescent: Impacts and associated atmospheric circulation. *Agric. For. Meteorol.* **2010**, *150*, 1245–1257.
31. Deininger, M.; McDermott, F.; Mudelsee, M.; Werner, M.; Frank, N.; Mangini, A. Coherency of late Holocene European speleothem δ18O records linked to North Atlantic Ocean circulation. *Clim. Dyn.* **2016**, 1–24.
32. Atsawawaranunt, K.; Comas-Bru, L.; Amirnezhad-Mozhdehi, S.; Deininger, M.; Harrison, S.P.; Baker, A.; Boyd, M.; Kaushal, N.; Ahmad, S.M.; Ait Brahim, Y.; et al. The SISAL database: a global resource to document oxygen and carbon isotope records from speleothems. *Earth Syst. Sci. Data Discuss.* **2018**, 1–

64.

33. Comas-Bru, L.; Harrison, S.P.; Deininger, M. SISAL, speleothems and the state-of-the-art. *Quaternary* **2019**, *107*, 7921–7925.
34. Baker, A.; Smith, C.L.; Jex, C.N.; Fairchild, I.J.; Genty, D.; Fuller, L. Annually Laminated Speleothems: a Review. *Int. J. Speleol.* **2008**, *37*, 193–206.
35. Fairchild, I.J.; Baker, A. *Speleothem science: from process to past environments*; John Wiley & Sons, 2012; Vol. 3;.
36. Chen, Z.; Auler, A.S.; Bakalowicz, M.; Drew, D.; Griger, F.; Hartmann, J.; Jiang, G.; Moosdorf, N.; Richts, A.; Stevanovic, Z.; et al. The World Karst Aquifer Mapping project: concept, mapping procedure and map of Europe. *Hydrogeol. J.* **2017**, *25*, 771–785.
37. Kern, Z.; Demény, A.; Hatvani, I.G. Speleothem stable isotope records from Eastern Europe & Turkey. **2019**.
38. McGregor, H. V.; Evans, M.N.; Goosse, H.; Leduc, G.; Martrat, B.; Addison, J.A.; Mortyn, P.G.; Oppo, D.W.; Seidenkrantz, M.S.; Sicre, M.A.; et al. Robust global ocean cooling trend for the pre-industrial Common Era. *Nat. Geosci.* **2015**, *8*, 671–677.
39. Emile-Geay, J.; McKay, N.P.; Kaufman, D.S.; von Gunten, L.; Wang, J.; Anchukaitis, K.J.; Abram, N.J.; Addison, J.A.; Curran, M.A.J.; Evans, M.N.; et al. A global multiproxy database for temperature reconstructions of the Common Era. *Sci. Data* **2017**, *4*, 170088.
40. Railsback, L.B.; Gibbard, P.L.; Head, M.J.; Voarintsoa, N.R.G.; Toucanne, S. An optimized scheme of lettered marine isotope substages for the last 1.0 million years, and the climatostratigraphic nature of isotope stages and substages. *Quat. Sci. Rev.* **2015**, *111*, 94–106.
41. Drăguşin, V.; Staubwasser, M.; Hoffmann, D.L.; Ersek, V.; Onac, B.P.; Veres, D. Constraining Holocene hydrological changes in the Carpathian-Balkan region using speleothem δ18O and pollen-based temperature reconstructions. *Clim. Past* **2014**, *10*, 1363–1380.
42. Kacanski, A.; Carmi, I.; Shemesh, A.; Kronfeld, J.; Yam, R.; Flexer, A. Late Holocene Climatic Change in the Balkans: Speleothem Isotopic Data from Serbia. *Radiocarbon* **2001**, *43*, 647–658.
43. Burns, S.J.; Fleitmann, D.; Mudelsee, M.; Neff, U.; Matter, A.; Mangini, A. A 780-year annually resolved record of Indian Ocean monsoon precipitation from a speleothem from south Oman. *J. Geophys. Res.* **2002**, *107*.
44. Fleitmann, D.; Burns, S.J.; Mangini, A.; Mudelsee, M.; Kramers, J.; Villa, I.; Neff, U.; Al-Subbary, A.A.; Buettner, A.; Hippler, D.; et al. Holocene ITCZ and Indian monsoon dynamics recorded in stalagmites from Oman and Yemen (Socotra). *Quat. Sci. Rev.* **2007**, *26*, 170–188.
45. Ünal-Imer, E.; Shulmeister, J.; Zhao, J.X.; Tonguç Uysal, I.; Feng, Y.-X.; Duc Nguyen, A.; Yüce, G. An 80 kyr-long continuous speleothem record from Dim Cave, SW Turkey with paleoclimatic implications for the Eastern Mediterranean. *Sci. Rep.* **2015**, *5*, 1–9.
46. Neff, U.; Burns, S.J.; Mangini, A.; Mudelsee, M.; Fleitmann, D.; Matter, A. Strong coherence between solar variability and the monsoon in Oman between 9 and 6 kyr ago. *Nature* **2001**, *411*, 290–293.
47. Burns, S.J.; Fleitmann, D.; Matter, A.; Neff, U.; Mangini, A. Speleothem evidence from Oman for continental pluvial events during interglacial periods. *Geology* **2001**, *29*, 623–626.
48. Cheng, H.; Sinha, A.; Verheyden, S.; Nader, F.H.; Li, X.L.; Zhang, P.-Z.; Yin, J.J.; Yi, L.; Peng, Y.B.; Rao, Z.G.; et al. The climate variability in northern Levant over the past 20,000 years. *Geophys. Res. Lett.* **2015**, *42*, 8641–8650.
49. Verheyden, S.; Nader, F.H.; Cheng, H.; Edwards, R.L.; Swennen, R. Paleoclimate reconstruction in the

Levant region from the geochemistry of a Holocene stalagmite from the Jeita cave, Lebanon. *Quat. Res.* **2008**, *70*, 368–381.

50. Frumkin, A.; Ford, D.C.; Schwarcz, H.P. Continental Oxygen Isotopic Record of the Last 170 , 000 Years in Jerusalem. *Quat. Res.* **1999**, *51*, 317–327.
51. Nehme, C.; Verheyden, S.; Noble, S.R.; Farrant, A.R.; Sahy, D.; Hellstrom, J.C.; Delannoy, J.J.; Claeys, P. Reconstruction of MIS 5 climate in the central Levant using a stalagmite from Kanaan Cave, Lebanon. *Clim. Past* **2015**, *11*, 1785–1799.
52. Finné, M.; Bar-Matthews, M.; Holmgren, K.; Sundqvist, H.S.; Liakopoulos, I.; Zhang, Q. Speleothem evidence for late Holocene climate variability and floods in Southern Greece. *Quat. Res. (United States)* **2014**, *81*, 213–227.
53. Finné, M.; Holmgren, K.; Shen, C.C.; Hu, H.M.; Boyd, M.; Stocker, S. Late bronze age climate change and the destruction of the mycenaean palace of nestor at pylos. *PLoS One* **2017**, *12*, 1–18.
54. Shakun, J.D.; Burns, S.J.; Fleitmann, D.; Kramers, J.; Matter, A.; Al-Subary, A.A. A high-resolution, absolute-dated deglacial speleothem record of Indian Ocean climate from Socotra Island, Yemen. *Earth Planet. Sci. Lett.* **2007**, *259*, 442–456.
55. Psomiadis, D.; Dotsika, E.; Albanakis, K.; Ghaleb, B.; Hillaire-Marcel, C. Speleothem record of climatic changes in the northern Aegean region (Greece) from the Bronze Age to the collapse of the Roman Empire. *Palaeogeogr. Palaeoclimatol. Palaeoecol.* **2018**, *489*, 272–283.
56. Fleitmann, D.; Cheng, H.; Badertscher, S.; Edwards, R.L.; Mudelsee, M.; Göktürk, O.M.; Fankhauser, A.; Pickering, R.; Raible, C.C.; Matter, A.; et al. Timing and climatic impact of Greenland interstadials recorded in stalagmites from northern Turkey. *Geophys. Res. Lett.* **2009**, *36*, 1–5.
57. Göktürk, O.M.; Fleitmann, D.; Badertscher, S.; Cheng, H.; Edwards, R.L.; Leuenberger, M.; Fankhauser, A.; Tüysüz, O.; Kramers, J. Climate on the southern Black Sea coast during the Holocene: Implications from the Sofular Cave record. *Quat. Sci. Rev.* **2011**, *30*, 2433–2445.
58. Badertscher, S.; Fleitmann, D.; Cheng, H.; Edwards, R.L.; Göktürk, O.M.; Zumbühl, A.; Leuenberger, M.; Tüysüz, O. Pleistocene water intrusions from the Mediterranean and Caspian seas into the Black Sea. *Nat. Geosci.* **2011**, *4*, 236–239.
59. Grant, K.M.; Rohling, E.J.; Bar-Matthews, M.; Ayalon, A.; Medina-Elizalde, M.; Ramsey, C.B.; Satow, C.; Roberts, A.P. Rapid coupling between ice volume and polar temperature over the past 50,000 years. *Nature* **2012**, *491*, 744–747.
60. Bar-Matthews, M.; Ayalon, A.; Kaufman, A. Late Quaternary Paleoclimate in the Eastern Mediterranean Region from Stable Isotope Analysis of Speleothems at Soreq Cave, Israel. *Quat. Res.* **1997**, *47*, 155–168.
61. Bar-Matthews, M.; Ayalon, A.; Kaufman, A. Middle to Late Holocene (6500 Years Period) Paleoclimate in The Eastern Mediterranean Region From Stable Isotopic Composition Of Speleothems From Soreq Cave, Israel. *Isot. Tech. Study Environ. Chang.* 1998, 673–682.
62. Bar-Matthews, M.; Ayalon, A.; Kaufman, A.; Wasserburg, G.J. The Eastern Mediterranean paleoclimate as a reflection of regional events: Soreq cave, Israel. *Earth Planet. Sci. Lett.* **1999**, *166*, 85–95.
63. Bar-Matthews, M.; Ayalon, A.; Kaufman, A. Timing and hydrological conditions of Sapropel events in the Eastern Mediterranean, as evident from speleothems, Soreq cave, Israel. *Chem. Geol.* **2000**, *169*, 145–156.
64. Ayalon, A.; Bar-Matthews, M.; Kaufman, A. Climatic conditions during marine oxygen isotope stage 6 in the eastern Mediterranean region from the isotopic composition of speleothems of Soreq Cave, Israel.

Geology **2002**, *30*, 303.

65. Schilman, B.; Ayalon, A.; Bar-Matthews, M.; Kagan, E.J.; Almogi-Labin, A. Sea-land paleoclimate correlation in the Eastern Mediterranean region during the late Holocene. *Isr. J. Earth Sci.* **2002**, *51*, 181–190.
66. Kolodny, Y.; Bar-Matthews, M.; Ayalon, A.; McKeegan, K.D. A high spatial resolution d18O profile of a speleothem using an ion-microprobe. *Chem. Geol.* **2003**, *197*, 21–28.
67. Bar-Matthews, M.; Ayalon, A.; Gilmour, M.A.; Matthews, A.; Hawkesworth, C.J. Sea–land oxygen isotopic relationships from planktonic foraminifera and speleothems in the Eastern Mediterranean region and their implication for paleorainfall during interglacial intervals. *Geochim. Cosmochim. Acta* **2003**, *67*, 3181–3199.
68. Jex, C.N.; Baker, A.; Fairchild, I.J.; Eastwood, W.J.; Leng, M.J.; Sloane, H.J.; Thomas, L.; Bekaroğlu, E. Calibration of speleothem δ18O with instrumental climate records from Turkey. *Glob. Planet. Change* **2010**, *71*, 207–217.
69. Van Rampelbergh, M.; Fleitmann, D.; Verheyden, S.; Cheng, H.; Edwards, R.L.; De Geest, P.; De Vleeschouwer, D.; Burns, S.J.; Matter, A.; Claeys, P.; et al. Mid- to late Holocene Indian Ocean Monsoon variability recorded in four speleothems from Socotra Island, Yemen. *Quat. Sci. Rev.* **2013**, *65*, 129–142.
70. Carolin, S.A.; Walker, R.T.; Henderson, G.M.; Maxfield, L.; Ersek, V.; Sloan, A.; Talebian, M.; Fattahi, M.; Nezamdoust, J. Decadal-scale Climate Variability on the Central Iranian Plateau Spanning the So-called 4.2 ka BP Drought Event. In Proceedings of the AGU Fall Meeting Abstracts; 2015.
71. Rowe, P.J.; Mason, J.E.; Andrews, J.E.; Marca, A.D.; Thomas, L.; Van Calsteren, P.; Jex, C.N.; Vonhof, H.B.; Al-Omari, S. Speleothem isotopic evidence of winter rainfall variability in northeast Turkey between 77 and 6 ka. *Quat. Sci. Rev.* **2012**, *45*, 60–72.
72. Mehterian, S.; Pourmand, A.; Sharifi, A.; Lahijani, H.A.K.; Naderi, M.; Swart, P.K. Reconstruction of Pleistocene Paleo-Hydrology and Climate Variations in Western Asia as Recorded in Speleothems from West-Central Iran. In Proceedings of the AGU Fall Meeting AbstractsFall Meeting; 2014.
73. Vaks, A.; Bar-Matthews, M.; Ayalon, A.; Matthews, A.; Frumkin, A.; Dayan, U.; Halicz, L.; Almogi-Labin, A.; Schilman, B. Paleoclimate and location of the border between Mediterranean climate region and the Saharo–Arabian Desert as revealed by speleothems from the northern Negev Desert, Israel. *Earth Planet. Sci. Lett.* **2006**, *249*, 384–399.
74. Ayalon, A.; Bar-Matthews, M.; Frumkin, A.; Matthews, A. Last Glacial warm events on Mount Hermon: the southern extension of the Alpine karst range of the east Mediterranean. *Quat. Sci. Rev.* **2013**, *59*, 43–56.
75. Mehterian, S.; Pourmand, A.; Sharifi, A.; Lahijani, H.A.K.; Naderi, M.; Swart, P.K. Speleothem records of glacial/interglacial climate from Iran forewarn of future Water Availability in the interior of the Middle East. *Quat. Sci. Rev.* **2017**, *164*, 187–198.
76. Rifai, R.I. Reconstruction of the Middle Pleistocene climate of south Mediterranean using the Wadi Sannur speleothem, eastern Desert, Egypt. *Carbonates and Evaporites* **2007**, *22*, 73–85.
77. Keinan, J. Paleo-environment of the Northern Jordan Rift region based on speleothems from Zalmon Cave , Hebrew University of Jerusalem, 2016.
78. Brayshaw, D.J.; Hoskins, B.; Black, E. Some physical drivers of changes in the winter storm tracks over the North Atlantic and Mediterranean during the Holocene. *Philos. Trans. R. Soc. A Math. Phys. Eng. Sci.* **2010**, *368*, 5185–5223.
79. Ulbrich, U.; Lionello, P.; Belušić, D.; Jacobeit, J.; Knippertz, P.; Kuglitsch, F.G.; Leckebusch, G.C.;

Luterbacher, J.; Maugeri, M.; Maheras, P.; et al. Climate of the Mediterranean: Synoptic Patterns, Temperature, Precipitation, Winds, and Their Extremes. In *The Climate of the Mediterranean Region: From The Past to the Future*; Lionello, P., Ed.; Elsevier, 2012; pp. 301–346.

80. Karaca, M.; Deniz, A.; Tayanç, M. Cyclone track variability over Turkey in association with regional climate. *Int. J. Climatol.* **2000**, *20*, 1225–1236.
81. Gat, J.R.; Klein, B.; Kushnir, Y.; Roether, W.; Wernli, H.; Yam, R.; Shemesh, A. Isotope composition of air moisture over the Mediterranean Sea: An index of the air-sea interaction pattern. *Tellus, Ser. B Chem. Phys. Meteorol.* **2003**, *55*, 953–965.
82. Alpert, P.; Neeman, B.U.; Shay-El, Y. Climatological analysis of Mediterranean cyclones using ECMWF data. *Tellus A Dyn. Meteorol. Oceanogr.* **1990**, *42*, 65–77.
83. Lionello, P.; Trigo, I.F.; Gil, V.; Liberato, M.L.R.; Nissen, K.M.; Pinto, J.G.; Raible, C.C.; Reale, M.; Tanzarella, A.; Trigo, R.M.; et al. Objective climatology of cyclones in the Mediterranean region: A consensus view among methods with different system identification and tracking criteria. *Tellus, Ser. A Dyn. Meteorol. Oceanogr.* **2016**, *68*.
84. Weyhenmeyer, C.E.; Burns, S.J.; Waber, H.N.; Aeschbach-Hertig, W.; Kipfer, R.; Loosli, H.H.; Matter, A. Cool glacial temperatures and changes in moisture source recorded in Oman groundwaters. *Science (80-.).* **2000**, *287*, 842–845.
85. Findlater, J. Interhemispheric transport of air in the lower troposphere over the western Indian Ocean. *J. R. Met. Soc* **1969**, *95*, 400–403.
86. Almazroui, M.; Nazrul Islam, M.; Athar, H.; Jones, P.D.; Rahman, M.A. Recent climate change in the Arabian Peninsula: Annual rainfall and temperature analysis of Saudi Arabia for 1978-2009. *Int. J. Climatol.* **2012**, *32*, 953–966.
87. Almazroui, M. The relationship between atmospheric circulation patterns and surface climatic elements in Saudi Arabia, University of East Anglia, 2006.
88. Gat, J.R.; Carmi, I. Effect of climate changes on the precipitation patterns and isotopic composition of water in a climate transition zone : Case of the Eastern Mediterranean Sea area. In Proceedings of the The Influence of Climate Chnage and Climatic Variability on the Hydrolic Regime and Water Resources; IAHS: Vancouver, 1987; pp. 513–524.
89. Ayalon, A.; Bar-Matthews, M.; Sass, E. Rainfall-recharge relationships within a karstic terrain in the Eastern Mediterranean semi-arid region , Israel: d180 and dD characteristics. *J. Hydrol.* **1998**, *207*, 18–31.
90. Goldsmith, Y.; Polissar, P.J.; Ayalon, A.; Bar-Matthews, M.; de Menocal, P.B.; Broecker, W.S. The modern and Last Glacial Maximum hydrological cycles of the Eastern Mediterranean and the Levant from a water isotope perspective. *Earth Planet. Sci. Lett.* **2017**, *457*, 302–312.
91. Gat, J.R.; Dansgaard, W. Stable isotope survey of the fresh water occurrences in Israel and the Northern Jordan Rift Valley. *J. Hydrol.* **1972**, *16*, 177–211.
92. Craig, H. Isotopic Variations in Meteoric Waters. *Science* **1961**, *133*, 1702–1703.
93. Bar-Matthews, M.; Ayalon, A.; Vaks, A.; Frumkin, A. Climate and Environment Reconstruction Based on Speleothems from the Levant. In *Quaternary of the Levant, Environments, Climate Change, and Humans*; Bar-Yosef, O., Enzel, Y., Eds.; Cambridge University Press, 2017; pp. 151–164 ISBN 9781316106754.
94. Bar-Yosef, O. On the Nature of Transitions: the Middle to Upper Palaeolithic and the Neolithic Revolution. *Cambridge Archaeol. J.* **1998**, *8*, 63–141.
95. Deininger, M.; Ward, B.M.; Novello, V.F.; Cruz, F.W. Late Quaternary Variations in the South American Monsoon System as Inferred by Speleothems – New Perspectives Using the SISAL Database. *Quaternary*

2018.

96. Orland, I.J.; Burstyn, Y.; Bar-Matthews, M.; Kozdon, R.; Ayalon, A.; Matthews, A.; Valley, J.W. Seasonal climate signals (1990–2008) in a modern Soreq Cave stalagmite as revealed by high-resolution geochemical analysis. *Chem. Geol.* **2014**, *363*, 322–333.
97. Ayalon, A.; Bar-Matthews, M.; Schilman, B. *Rainfall Isotopic Characteristics At Vatious Sites In Israel And The Relationships With Unsaturated Zone Water*; 04; The Geological Survey of Israel: Jerusalem, 2004; Vol. GSI/16/04;
98. Burstyn, Y. *Multi-decade to Seasonal Climate Change Recorded by Stable Isotope and Trace Element Variability in Modern Cave-waters and Calcite of Soreq Cave, Israel*; Jerusalem, 2013;
99. Kaufman, A.; Bar-Matthews, M.; Ayalon, A.; Carmi, I. The vadose flow above Soreq Cave, Israel: a tritium study of the cave waters. *J. Hydrol.* **2003**, *273*, 155–163.
100. Bar-Matthews, M.; Ayalon, A.; Matthews, A.; Sass, E.; Halicz, L. Carbon and oxygen isotope study of the active water-carbonate system in a karstic Mediterranean cave: Implications for paleoclimate research in semiarid regions. *Geochim. Cosmochim. Acta* **1996**, *60*, 337–347.
101. Kolodny, Y.; Stein, M.; Machlus, M. Sea-rain-lake relation in the Last Glacial East Mediterranean revealed by d18O-d13C in Lake Lisan aragonites. *Geochim. Cosmochim. Acta* **2005**, *69*, 4045–4060.
102. Almogi-Labin, A.; Bar-Matthews, M.; Shriki, D.; Kolosovsky, E.; Paterne, M.; Schilman, B.; Ayalon, A.; Aizenshtat, Z.; Matthews, A. Climatic variability during the last ~90 ka of the southern and northern Levantine Basin as evident from marine records and speleothems. *Quat. Sci. Rev.* **2009**, *28*, 2882–2896.
103. Cheng, H.; Sinha, A.; Wang, X.; Cruz, F.W.; Edwards, R.L. The Global Paleomonsoon as seen through speleothem records from Asia and the Americas. *Clim. Dyn.* **2012**, *39*, 1045–1062.
104. Ziegler, M.; Tuenter, E.; Lourens, L.J. The precession phase of the boreal summer monsoon as viewed from the eastern Mediterranean (ODP Site 968). *Quat. Sci. Rev.* **2010**, *29*, 1481–1490.
105. Rasmussen, S.O.; Bigler, M.; Blockley, S.P.; Blunier, T.; Buchardt, S.L.; Clausen, H.B.; Cvijanovic, I.; Dahl-Jensen, D.; Johnsen, S.J.; Fischer, H.; et al. A stratigraphic framework for abrupt climatic changes during the Last Glacial period based on three synchronized Greenland ice-core records: Refining and extending the INTIMATE event stratigraphy. *Quat. Sci. Rev.* **2014**, *106*, 14–28.
106. Büntgen, U.; Myglan, V.S.; Ljungqvist, F.C.; McCormick, M.; Di Cosmo, N.; Sigl, M.; Jungclaus, J.; Wagner, S.; Krusic, P.J.; Esper, J.; et al. Cooling and societal change during the Late Antique Little Ice Age from 536 to around 660 AD. *Nat. Geosci.* **2016**, *9*, 231–236.
107. Wanner, H.; Beer, J.; Bütikofer, J.; Crowley, T.J.; Cubasch, U.; Flückiger, J.; Goosse, H.; Grosjean, M.; Joos, F.; Kaplan, J.O.; et al. Mid- to Late Holocene climate change: an overview. *Quat. Sci. Rev.* **2008**, *27*, 1791–1828.
108. Drăguşin, V.; Staubwasser, M.; Hoffmann, D.L.; Ersek, V.; Onac, B.P.; Veres, D. Constraining Holocene hydrological changes in the Carpathian-Balkan region using speleothem δ18O and pollen-based temperature reconstructions. *Clim. Past* **2014**, *10*, 1363–1380.
109. Finné, M.; Bar-Matthews, M.; Holmgren, K.; Sundqvist, H.S.; Liakopoulos, I.; Zhang, Q. Speleothem evidence for late Holocene climate variability and floods in Southern Greece. *Quat. Res.* **2014**, *81*, 213–227.
110. Box, M.R.; Krom, M.D.; Cliff, R.A.; Bar-Matthews, M.; Almogi-Labin, A.; Ayalon, A.; Paterne, M. Response of the Nile and its catchment to millennial-scale climatic change since the LGM from Sr isotopes and major elements of East Mediterranean sediments. *Quat. Sci. Rev.* **2011**, *30*, 431–442.
111. Siani, G.; Magny, M.; Paterne, M.; Debret, M.; Fontugne, M. Paleohydrology reconstruction and

Holocene climate variability in the South Adriatic Sea. *Clim. Past* **2013**, *9*, 499–515.

112. Issar, A.S.; Zohar, M. *Climate change — Environment and history of the near east*; Springer Berlin Heidelberg: Berlin, Heidelberg, 2007; ISBN 9783540698517.
113. Abram, N.J.; McGregor, H. V.; Tierney, J.E.; Evans, M.N.; McKay, N.P.; Kaufman, D.S.; Consortium, the P. 2k; Thirumalai, K.; Martrat, B.; Goosse, H.; et al. Early onset of industrial-era warming across the oceans and continents. *Nature* **2016**, *536*, 411–418.
114. Vinther, B.M.; Buchardt, S.L.; Clausen, H.B.; Dahl-Jensen, D.; Johnsen, S.J.; Fisher, D.A.; Koerner, R.M.; Raynaud, D.; Lipenkov, V.; Andersen, K.K.; et al. Holocene thinning of the Greenland ice sheet. *Nature* **2009**, *461*, 385–388.
115. Jalali, B.; Sicre, M.-A.; Bassetti, M.-A.; Kallel, N. Holocene climate variability in the North-Western Mediterranean Sea (Gulf of Lions). *Clim. Past* **2016**, *12*, 91–101.
116. Martrat, B.; Jimenez-Amat, P.; Zahn, R.; Grimalt, J.O. Similarities and dissimilarities between the last two deglaciations and interglaciations in the North Atlantic region. *Quat. Sci. Rev.* **2014**, *99*, 122–134.
117. Wunsch, C. Abrupt climate change: An alternative view. *Quat. Res.* **2006**, *65*, 191–203.
118. Bond, G.; Kromer, B.; Beer, J.; Muscheler, R.; Evans, M.N.; Showers, W.; Hoffmann, S.; Lotti-Bond, R.; Hajdas, I.; Bonani, G. Persistent solar influence on North Atlantic climate during the Holocene. *Science* **2001**, *294*, 2130–6.
119. Alley, R.B. Abrupt Climate Change. *Science (80-.).* **2003**, *299*, 2005–2010.
120. Stocker, T.F. Past and future reorganizations in the climate system. *Quat. Sci. Rev.* **2000**, *19*, 301–319.
121. Walker, M.; Johnsen, S.; Rasmussen, S.O.; Popp, T.; Steffensen, J.P.; Gibbard, P.; Hoek, W.; Lowe, J.; Andrews, J.; Björck, S.; et al. Formal definition and dating of the GSSP (Global Stratotype Section and Point) for the base of the Holocene using the Greenland NGRIP ice core, and selected auxiliary records. *J. Quat. Sci.* **2009**, *24*, 3–17.
122. Head, M.J.; Gibbard, P.L. Formal subdivision of the Quaternary System/Period: Past, present, and future. *Quat. Int.* **2015**, *383*, 4–35.
123. Kleiven, H.K.F.; Kissel, C.; Laj, C.; Ninnemann, U.S.; Richter, T.O.; Cortijo, E. Reduced North Atlantic deep water coeval with the glacial Lake Agassiz freshwater outburst. *Science* **2008**, *319*, 60–4.
124. Thomas, E.R.; Wolff, E.W.; Mulvaney, R.; Steffensen, J.P.; Johnsen, S.J.; Arrowsmith, C.; White, J.W.C.; Vaughn, B.; Popp, T. The 8.2 ka event from Greenland ice cores. *Quat. Sci. Rev.* **2007**, *26*, 70–81.
125. Wu, C.J.; Usoskin, I.G.; Krivova, N.; Kovaltsov, G.A.; Baroni, M.; Bard, E.; Solanki, S.K. Solar activity over nine millennia: A consistent multi-proxy reconstruction. *Astron. Astrophys.* **2018**, *615*, A93.
126. Zielinski, G.A.; Mayewski, P.A.; Meeker, L.D.; Grönvold, K.; Germani, M.S.; Whitlow, S.; Twickler, M.S.; Taylor, K. Volcanic aerosol records and tephrochronology of the Summit, Greenland, ice cores. *J. Geophys. Res. Ocean.* **1997**, *102*, 26625–26640.
127. Rohling, E.J. Review and new aspects concerning the formation of eastern Mediterranean sapropels. *Mar. Geol.* **1994**, *122*, 1–28.
128. Lange, D.; Gert, J.; Thomson, J.; Reitz, A.; Slomp, C.P.; Principato, M.S.; Erba, E.; Corselli, C. Synchronous basin-wide formation and redox-controlled preservation of a Mediterranean sapropel. **2008**, *1*.
129. Rohling, E.J.; Marino, G.; Grant, K.M. Mediterranean climate and oceanography, and the periodic development of anoxic events (sapropels). *Earth-Science Rev.* **2015**, *143*, 62–97.
130. Grant, K.M.; Grimm, R.; Mikolajewicz, U.; Marino, G.; Ziegler, M.; Rohling, E.J. The timing of Mediterranean sapropel deposition relative to insolation, sea-level and African monsoon changes. *Quat.*

Sci. Rev. **2016**, *140*, 125–141.

131. de Menocal, P.B.; Ortiz, J.; Guilderson, T.; Adkins, J.; Sarnthein, M.; Baker, L.; Yarusinsky, M. Abrupt onset and termination of the African Humid Period:: rapid climate responses to gradual insolation forcing. *Quat. Sci. Rev.* **2000**, *19*, 347–361.
132. de Menocal, P.B. Palaeoclimate: End of the African Humid Period. *Nat. Geosci.* **2015**, *8*, 86–87.
133. González-Sampériz, P.; Utrilla, P.; Mazo, C.; Valero-Garcés, B.; Sopena, M.; Morellón, M.; Sebastián, M.; Moreno, A.; Martínez-Bea, M. Patterns of human occupation during the early Holocene in the Central Ebro Basin (NE Spain) in response to the 8.2 ka climatic event. *Quat. Res.* **2009**, *71*, 121–132.
134. García-Martínez de Lagrán, I.; Iriarte, E.; García-Gazólaz, J.; Tejedor-Rodríguez, C.; Gibaja-Bao, J.F.; Moreno-García, M.; Pérez-Jordà, G.; Ruiz-Alonso, M.; Sesma-Sesma, J.; Garrido-Pena, R.; et al. 8.2 ka BP paleoclimatic event and the Ebro Valley Mesolithic groups: Preliminary data from Artusia rock shelter (Unzué, Navarra, Spain). *Quat. Int.* **2016**, *403*, 151–173.
135. Torfstein, A.; Goldstein, S.L.; Stein, M.; Enzel, Y. Impacts of abrupt climate changes in the Levant from Last Glacial Dead Sea levels. *Quat. Sci. Rev.* **2013**, *69*, 1–7.
136. Renssen, H.; Brovkin, V.; Fichefet, T.; Goosse, H. Simulation of the Holocene climate evolution in Northern Africa: The termination of the African Humid Period. *Quat. Int.* **2006**, *150*, 95–102.
137. Shanahan, T.M.; McKay, N.P.; Hughen, K.A.; Overpeck, J.T.; Otto-Bliesner, B.; Heil, C.W.; King, J.; Scholz, C.A.; Peck, J. The time-transgressive termination of the African Humid Period. *Nat. Geosci.* **2015**, *8*, 140–144.
138. Kuper, R.; Kröpelin, S. Climate-Controlled Holocene Occupation in the Sahara: Motor of Africa's Evolution. *Science (80-.).* **2006**, *313*, 803–807.
139. Kröpelin, S.; Verschuren, D.; Lézine, A.-M.; Eggermont, H.; Cocquyt, C.; Francus, P.; Cazet, J.-P.; Fagot, M.; Rumes, B.; Russell, J.M.; et al. Climate-driven ecosystem succession in the Sahara: the past 6000 years. *Science* **2008**, *320*, 765–8.
140. Carolin, S.A.; Walker, R.T.; Day, C.C.; Ersek, V.; Sloan, R.A.; Dee, M.W.; Talebian, M.; Henderson, G.M. Precise timing of abrupt increase in dust activity in the Middle East coincident with 4.2 ka social change. *Proc. Natl. Acad. Sci. U. S. A.* **2019**, *116*, 67–72.
141. Nicholson, S.E.; Nash, D.J.; Chase, B.M.; Grab, S.W.; Shanahan, T.M.; Verschuren, D.; Asrat, A.; Lézine, A.M.; Umer, M. Temperature variability over Africa during the last 2000 years. *Holocene* **2013**, *23*, 1085–1094.
142. Luterbacher, J.; Pfister, C. The year without a summer. *Nat. Geosci. 2015 84* **2015**.
143. Zhang, D.D.; Lee, H.F.; Wang, C.; Li, B.; Pei, Q.; Zhang, J.; An, Y. The causality analysis of climate change and large-scale human crisis. *Proc. Natl. Acad. Sci. U. S. A.* **2011**, *108*, 17296–301.
144. Alonso-Garcia, M.; Kleiven, H. (Kikki) F.; McManus, J.F.; Moffa-Sanchez, P.; Broecker, W.S.; Flower, B.P. Freshening of the Labrador Sea as a trigger for Little Ice Age development. *Clim. Past* **2017**, *13*, 317–331.
145. Moreno-Chamarro, E.; Zanchettin, D.; Lohmann, K.; Luterbacher, J.; Jungclaus, J.H. Winter amplification of the European Little Ice Age cooling by the subpolar gyre. *Sci. Rep.* **2017**, *7*, 9981.
146. Dezileau, L.; Sabatier, P.; Blanchemanche, P.; Joly, B.; Swingedouw, D.; Cassou, C.; Castaings, J.; Martinez, P.; Von Grafenstein, U. Intense storm activity during the Little Ice Age on the French Mediterranean coast. *Palaeogeogr. Palaeoclimatol. Palaeoecol.* **2011**, *299*, 289–297.
147. Levine, X.J.; Schneider, T.; Levine, X.J.; Schneider, T. Baroclinic Eddies and the Extent of the Hadley Circulation: An Idealized GCM Study. *J. Atmos. Sci.* **2015**, *72*, 2744–2761.

148. Gao, C.; Robock, A.; Ammann, C. Volcanic forcing of climate over the past 1500 years: An improved ice core-based index for climate models. *J. Geophys. Res.* **2008**, *113*, D23111.

149. Marsh, A.; Fleitmann, D.; Al-Manmi, D.A.M.; Altaweel, M.; Wengrow, D.; Carter, R. Mid- to late-Holocene archaeology, environment and climate in the northeast Kurdistan region of Iraq. *The Holocene* **2018**, *28*, 955–967.

150. Wassenburg, J.A.; Dietrich, S.; Fietzke, J.; Fohlmeister, J.; Jochum, K.P.; Scholz, D.; Richter, D.K.; Sabaoui, A.; Spötl, C.; Lohmann, G.; et al. Reorganization of the North Atlantic Oscillation during early Holocene deglaciation. *Nat. Geosci.* **2016**, *9*, 602–605.

151. Deininger, M.; Werner, M.; McDermott, F. North Atlantic Oscillation controls on oxygen and hydrogen isotope gradients in winter precipitation across Europe; Implications for palaeoclimate studies. *Clim. Past* **2016**, *12*, 2127–2143.

152. Hurrell, J.W. Decadal Trends in the North Atlantic Oscillation: Regional Temperatures and Precipitation. *Science (80-.).* **1995**, *269*, 676–679.

153. Braun, K.; Nehme, C.; Pickering, R.; Rogerson, M.; Scroxton, N. A Window into Africa's Past Hydroclimates: The SISAL_V1 Database Contribution. *Quaternary* **2018**.